Inorganic Solid-State Electrolytes for Lithium Batteries: Mechanisms and Properties Governing Ion Conduction

Citation: Bachman, John Christopher, Sokseiha Muy, Alexis Grimaud, Hao-Hsun Chang, Nir Pour, Simon F. Lux, Odysseas Paschos, et al. “Inorganic Solid-State Electrolytes for Lithium Batteries: Mechanisms and Properties Governing Ion Conduction.” Chemical Reviews 116, no. 1 (January 13, 2016): 140–162.

Published Version: http://dx.doi.org/10.1021/acs.chemrev.5b00563

Publisher: American Chemical Society (ACS)

Permanent Link: http://hdl.handle.net/1721.1/109539

Version: Author's final manuscript: final author’s manuscript post peer review, without publisher’s formatting or copy editing

A Review of Inorganic Solid-State Electrolytes for Lithium Batteries: Mechanisms and Properties Governing Ion Conduction

John Christopher Bachman[1,2,‡], Sokseiha Muy[1,3,‡], Alexis Grimaud[1,4,‡], Hao-Hsun Chang[1,4], Nir Pour[1,4], Simon F. Lux[5], Odysseas Paschos[6], Filippo Maglia[6], Saskia Lupart[6], Peter Lamp[6], Livia Giordano[1,4,7] and Yang Shao-Horn[1,2,3,4] ∗

[1]Electrochemical Energy Laboratory, [2]Department of Mechanical Engineering, [3]Department of Materials Science and Engineering, [4]Research Laboratory of Electronics, Massachusetts Institute of Technology, Cambridge, Massachusetts 02139, United States

[5]BMW Group Technology Office USA, Mountain View, California 94043, United States

[6]BMW Group, Research Battery Technology, Munich, 80788, Germany

[7]Dipartimento di Scienza dei Materiali, Università di Milano-Bicocca, Milano, Italy

‡ These authors contributed equally

*email: shaohorn@mit.edu

A.G. current address: Chimie du Solide et Energie, FRE 3677, Collège de France, 75231 Paris Cedex 05, France or Réseau sur le Stockage Electrochimique de l'Energie (RS2E), FR CNRS 3459, 80039 Amiens Cedex, France

Abstract

This review article is focused on ion-transport mechanisms and fundamental properties of solid-state electrolytes to be used in electrochemical energy storage systems. Properties of the migrating species significantly affecting diffusion, including the valency and ionic radius, are discussed. The nature of the ligand and metal composing the skeleton of the host framework are analyzed and shown to have large impacts on the performance of solid-state electrolytes. A comprehensive identification of the candidate migrating species and structures is carried out. Not only the bulk properties of the conductors are explored, but the concept of tuning the conductivity through interfacial effects—specifically controlling grain boundaries and strain at the interfaces—is introduced. High-frequency dielectric constants and frequencies of low-energy optical phonons are shown as examples of properties than correlate with activation energy across many classes of ionic conductors. Experimental studies and theoretical results are discussed in parallel to give a pathway for further improvement of solid-state electrolytes. Through this discussion, the present review aims to provide insight into the physical parameters affecting the diffusion process, to allow for a more efficient and target-oriented research on improving solid-state ion conductors.

Table of Contents

1. Introduction: Applications of Solid-State Electrolytes

Solid-state inorganic electrolytes enable a number of emerging technologies ranging from solid oxide fuel cells,[1] smart windows,[2] sensors,[3,4] memristors,[5] microbatteries for on-chip power[6] and solid-state batteries for electrical vehicles.[7] While it is well known that silver-[8,9] and sodium-[10,11] ion conductors can have ionic conductivities comparable to that of liquid electrolytes,[12] recent breakthroughs have led to marked increases in lithium-ion conductivity. Considerable research has focused on a number of crystal structures including LISICON-like (lithium superionic conductor),[13] argyrodites,[14] garnets,[15] NASICON-like (sodium superionic conductor),[16] lithium nitrides,[17,18] lithium hydrides,[19] perovskites[20,21] and lithium halides,[22] where increasing conductivities can be achieved by structural and compositional tuning within a given family of structures. Lithium-ion conductivities in the argyrodites,[14] thio-LISICON[23] as well as the $Li_{10}MP_2S_{12}$ (LMPS) (M = Si, Ge, Sn)[24-26] structures are approaching that of liquid electrolytes such as ethylene carbonate: dimethyl carbonate with 1 M $LiPF_6$ ~ 10^{-2} S/cm, shown in Figure 1.[27] These lithium-ion conductors provide exciting opportunities in the development of solid-state lithium-ion and lithium-air batteries for vehicle applications. Replacing the aprotic electrolytes used in current lithium-ion batteries[7,28-30] by these solid-state electrolytes can lead to transformative advances in electrode concentration polarization due to: the high lithium transference number of solid-state electrolytes (~1) compared to aprotic electrolytes (0.2-0.5),[31,32] increased lithium-ion battery lifetime and safety[33-37] due to the greater electrochemical stability voltage window,[31,38-40] enhanced thermal stability,[37,41] and diminished flammability.[37,42] The enhanced stability and safety of solid-state inorganic electrolytes provides opportunities to simplify and redesign safety measures currently used in the battery cell, for example overpressure vents or charge interruption devices as well as sophisticated thermal management systems or constraints in the operational strategy in the battery pack.

While many solid-state electrolytes are found to have a wide electrochemical stability window, there are still numerous fast ion conductors reported to date that are unstable at low potentials against negative electrodes such as graphite and metallic lithium,[43] requiring the use of electrode materials such as

titanates to be used.[44] Fast ion conductors can also react with positive electrode materials, resulting in low interfacial charge transfer kinetics.[36,37] Although structural tuning by substitution within a given structural family can enhance lithium-ion conductivity, there is lack of fundamental understanding to establish a universal guide for fast ion conductors among different structural families. Thus it is not straightforward to predict the most conducting structure/composition, which limits the design of new or multi-layer lithium-ion conductors with enhanced conductivity and stability in order to meet all the requirements of solid-state lithium-ion batteries. Therefore, further studies in the lithium-ion conductivity trends and mechanisms among different classes of ion conductors are needed to provide insights into universal descriptors of lithium-ion conductivity, and aid the design of advanced lithium-ion conductors.

In this review, we survey previous research to search for key physical parameters that have been found to have a large influence on the ionic conductivities of crystalline solids, with emphasis on solid-state inorganic lithium conductors. While previous reviews report detailed structures and conductivities for each class of solid electrolytes[45] or focus on a specific family such as lanthanide oxides,[12] perovskites[20,21] and garnets[15] for instance, we aim to provide researchers new insights into correlating lithium-conductivity with lattice volume or diffusion bottleneck sizes across several well-known structural families, and opportunities in developing universal descriptors governing ionic conductivity and using interfaces/sizes to design next-generation solid-state electrolytes for lithium batteries.

We first survey ions that are reported mobile in solid-state conductors, and cations and ligands that are used in the structure of solid-state conductors. We show that monovalent ions have the highest diffusion coefficients and lowest migration energies by comparing diffusion coefficients of M^+ (Li^+, Na^+, K^+ etc), M^{2+} (Mg^{2+}, Ca^{2+}, Zn^{2+}, Cd^{2+} etc) and M^{3+} (Tm^{3+} and Al^{3+}) in Li_2SO_4 at 550 ^oC. In addition, by examining the trends found in the diffusion coefficients and migration energies of monovalent cations in β-alumina at 440 ^oC, we discuss that the highest diffusion coefficient and lowest migration energies can be obtained for monovalent ions whose sizes are not too small nor too large for a given structure. Moreover, even though higher ionic conductivity can be obtained by increasing the concentration of mobile ions and/or lowering

the energy of migration, these two parameters cannot be decoupled, which limits the maximum ionic conductivity and highlights current challenges in lithium-ion conductor research.

Second, we show that there are a number of structural families that exhibit high lithium-ion conductivities in the range of 10^{-2} to 10^{-3} S/cm at room temperature, and lithium-ion conductivity can vary greatly by up to 5-6 orders of magnitude within each family. Of significance, we highlight that increasing the lattice volume or lithium-ion diffusion bottleneck size has been exploited effectively to enhance lithium-ion conductivity in LISCON-like, NASICON-like, and perovskites while disordering lithium in tetrahedral and octahedral sites is essential to achieve high lithium-ion conductivity in the garnet structure.

Third, we discuss opportunities in establishing the volume of the diffusion pathway and parameters of lattice dynamics such as low-energy phonon frequency as universal descriptors for conduction of lithium and other ions among different structural families. Lastly, we show opportunities in exploiting size-tailored space charge regions to develop highly conducting nanostructured lithium-ion conductors.

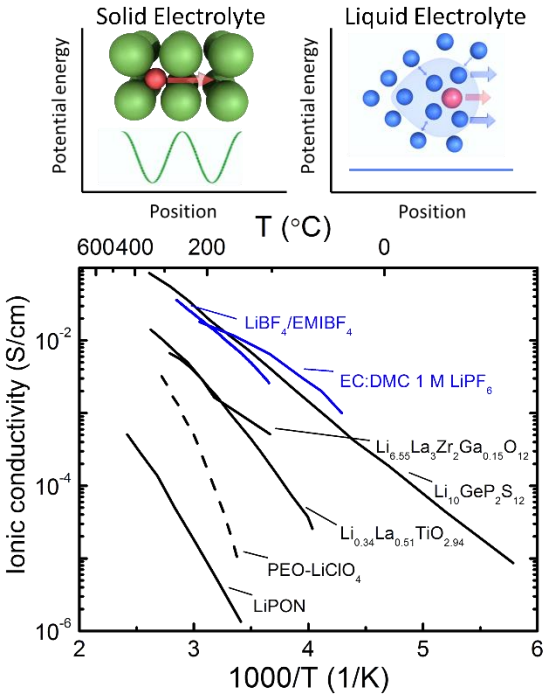

Figure 1. Reported total lithium-ion conductivity (unless otherwise mentioned) as a function of temperature adapted from Kamaya et al.,[24] which includes liquid (blue) EC:DMC 1 M $LiPF_6$[27] and ionic liquid $LiBF_4$ /$EMIBF_4$;[46] polymer (dashed black) PEO-$LiClO_4$,[47] inorganic solids (black) consisting of amorphous LiPON[48] and crystalline solids: perovskite $Li_{0.34}La_{0.51}TiO_{2.94}$ (bulk conductivity shown),[49] garnet $Li_{6.55}La_3Zr_2Ga_{0.15}O_{12}$[50] and $Li_{10}GeP_2S_{12}$.[24] Top right and top left show the potential energy of migration in liquid electrolytes of charged species in red with a solvation shell of electrolyte molecules (highlighted in blue) and an interstitial mobile ion in a crystalline solid, respectively.

2. Fundamentals of Solid-State Ion Conductors

2.1. Known Chemistry of Solid-State Ion Conductors

Solid-state ion conductors consist of mobile ions, and metal and non-metal ions which typically form polyhedra with ligands that create the skeleton of the crystal structure. More than half of the elements in the periodic table have been exploited in solid-state conductors to date. A number of cations and anions have shown to be mobile in solids including Li^+, Na^+, Cu^+, Ag^+, Mg^{2+}, F^- and O^{2-}, and are blue in Figure 2. One of the first solid-state conductors with a high-ionic conductivity was AgI,[8] which was followed by the development of sodium-ion conducting β-alumina[51] and NASICON[10], and then several fast lithium-ion conductors. Very recent works have suggested that divalent cations, for example, Mg^{2+} in mixed electron- and ion-conducting $Mg_xMo_6T_8$ (T being S or Se)[52] and ion-conducting $Mg(BH_4)(NH_2)$,[53] can have reasonable mobility in solids. Several anionic species can also be mobile in halides[54,55] and oxides[12] such as oxygen-ion conductors at elevated temperatures. A large number of metal and non-metal ions have been used for the skeleton of the polyhedral network, while chalcogens, halogens and nitrogen are used as ligands, as shown in green and red in Figure 2, respectively. Early transition-metal ions in the first and second row such as Ti^{4+}, Zr^{4+}, Nb^{5+} or Ta^{5+}, (which are $[Ne]3s^23p^63d^0$ and have no electrons in d-orbitals and thus do not have significant electronic conductivity) and ions from group 13 (e.g. Al^{3+} and Ga^{3+}) and 14 (e.g. Si^{4+} and Ge^{4+}), and 15 (e.g. P^{5+}) are used to create polyhedra in 12-fold, 8-fold, 6-fold or 4-fold coordination with the ligand. To form the backbone of the crystals, these polyhedra can be organized in

different ways, for example, by ordering into isolated polyhedral units as in γ-Li_3PO_4, by corner sharing as in NASICON, or by edge/corner sharing as in garnets. Details on these lithium conductors will be presented in later sections. These polyhedra can also be present in amorphous solids, but will lack the long-range ordering found in crystalline materials, one example being amorphous lithium phosphorus oxynitride.[56] Although amorphous solids are promising ion conductors,[57] in this review we will focus on crystalline materials and the information they provide on the diffusion process in solid-state electrolytes.

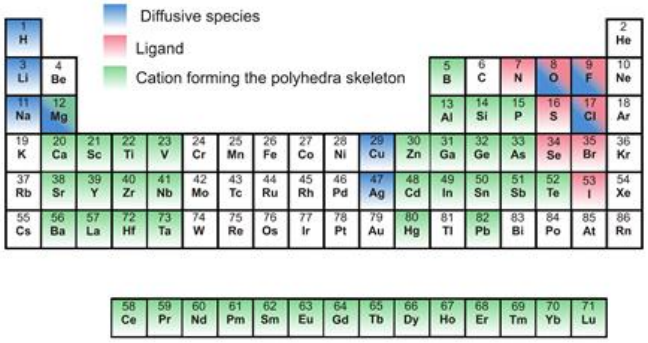

Figure 2. Periodic table with mobile ions in blue, ligands in red, and cations that can be used to build crystal structures to provide ionic conduction in green.

Both ion valency and size can greatly influence ionic conductivity in crystalline solids. Because of the increased electrostatic interactions between mobile ions and cations forming the structural skeleton, ionic conductivity and diffusivity decrease with increasing valency. The valency effect on the diffusion coefficient of monovalent, divalent and trivalent ions is well illustrated in Li_2SO_4 and aliovalent-substituted lithium sulfates at 550 ^oC.[58,59] The diffusion coefficient can decrease by three orders of magnitude from monovalent to trivalent ions in lithium sulfates, which is accompanied with considerable increase in the migration energy, as shown in Figure 3a and 3b, respectively. It is not surprising to note that ion conductors of monovalent ions such as silver ions, sodium ions and lithium ions have the highest conductivities reported to date. In contrast, a similar trend in the diffusion coefficient as a function of valency is noted for

these ions in aqueous solutions at room temperature in Figure 3a but the dependence on valency is much weaker as a result of a different ion-conduction mechanism from those in crystalline solids.[60]

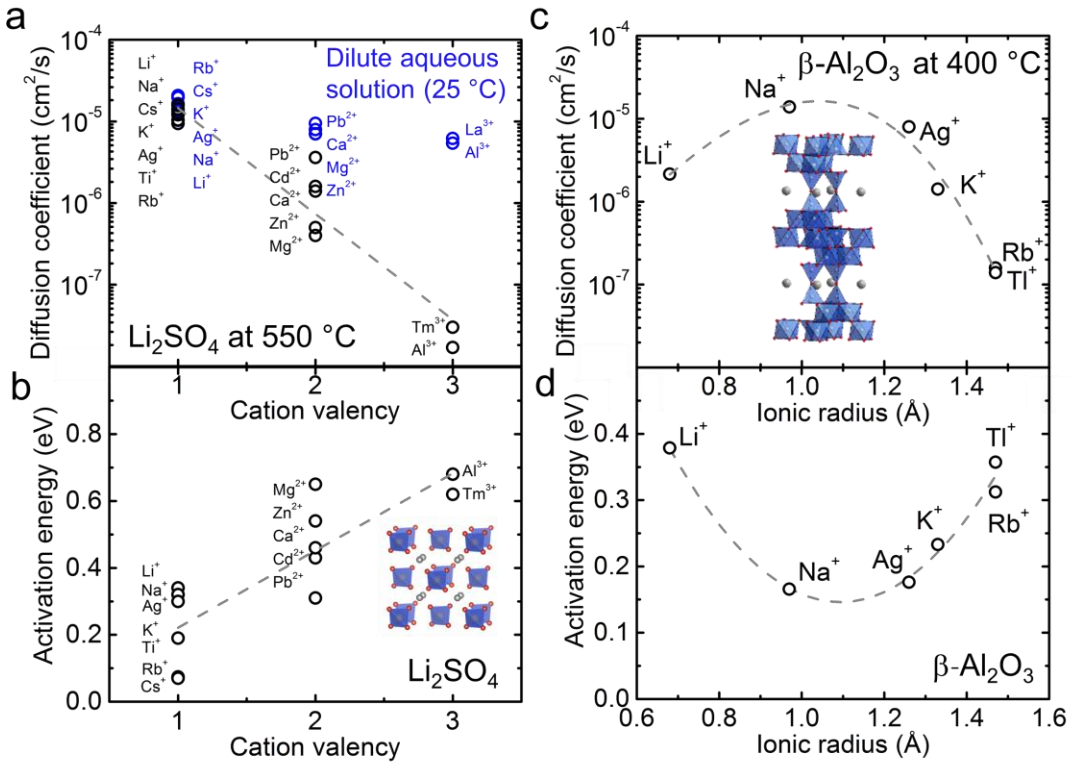

Figure 3. a) Reported cationic diffusion coefficients of monovalent, divalent and trivalent ions in Li_2SO_4 at 550 ˚C as a function of cation valency.[58] The diffusion coefficients of these ions in aqueous solutions at 25 ˚C are also included for comparison.[59] b) Activation energies for cation migration in Li_2SO_4.[58] c) Diffusion coefficients of monovalent ions in substituted β-alumina at 400 ˚C and d) activation energies for cations as a function of ionic radius.[61]

In addition to the migrating ion's valency, ionic size can greatly change the ionic conductivity. As shown in Figure 3a and 3b, considerable spread is noted for diffusion coefficients and activation energies for monovalent, divalent and trivalent ions with identical valencies. For instance, Pb^{2+} diffusion is an order of magnitude larger than the Mg^{2+} diffusion in Li_2SO_4 (Figure 3a) and the activation energy is ~ 2 times

smaller (Figure 3b). Interestingly, the dependence of diffusivity on the ionic radius, in many cases, is not monotonic[58,61] in contrast to reduced diffusivity with increasing valency. For example, the optimum ion size (sodium ions) gives rise to the highest diffusivity and lowest migration energy for monovalent ions for a given structure (β-alumina), as shown in Figure 3c and 3d, respectively. The highest diffusivities can be obtained for ions that are not too small nor too large for a given structure.[61] When the mobile cation is too small, the cation occupies a site with a large electrostatic well, which contains closer near-neighboring counterions, resulting in high activation energies and slow diffusion. On the other hand, when the mobile cation becomes too large, the cation experiences larger forces when diffusing between the bottlenecks of the skeleton structure, yielding reduced diffusivities and large migration energies. Therefore, design of fast lithium-ion conductors, on which we focus the review, requires understanding on how to tune the crystal structures to obtain optimum site sizes and diffusion channels for lithium diffusion, which will be discussed in the section 3.

2.2. Ion-Transport Mechanisms and Properties

The ion-conduction mechanisms in solid-state conductors are significantly different from liquid electrolytes. We focus our discussion on comparing lithium conduction in crystalline solids with aprotic electrolytes. Lithium-ion transport in aprotic liquid electrolytes involves moving solvated lithium ions in the solvent medium.[31] The lithium-ion conductivity in aprotic electrolytes can be enhanced by increasing salt/ion dissociation in solvents with greater dielectric constants, and promoting the mobility of solvated ions by lowering the viscosity of solvents via the Stokes-Einstein equation.[31] Due to reasonably fast exchange between the solvating molecules and the solvent molecules and uniform surroundings, the potential energy profile of mobile lithium ions in aprotic electrolytes can be considered flat (Figure 1, top right). In contrast, the diffusion of mobile species in a crystalline solid need to pass through periodic bottleneck points, which define an energetic barrier that separates the two local minima (typically

crystallographic sites for lithium) along the minimum energy pathway[62,63] (Figure 1, top left). This energy barrier, which is often referred to migration or motional energy, E_m, greatly influences ionic mobility and ionic conductivity, where low activation energy leads to high ionic mobility and conductivity.

The ionic conductivity of crystalline solids is also dependent on the amount of interstitials, vacancies and partial occupancy on lattice sites or interstices, which is determined by the ionic energy gap or defect formation energy, E_f, in stoichiometric ion conductors (known as the intrinsic regime). In addition, interstitials and vacancies can be created by substitution of aliovalent cations, whose formation energetics is governed by the trapping energy, E_t (known as extrinsic regime).[63] In both intrinsic and extrinsic regimes, the apparent activation energy E_A of ion conductivity contains both contributions from the defect formation energy E_f or E_t, and migration energy E_m (see supplementary information for examples types of defects).

Lithium-ion conductivity in a crystalline solid can be described by the product of the number of mobile lithium ions per unit volume, the square of the charge of each lithium ion and the absolute mobility of lithium ions. Considering non-interacting lithium ions, the lithium-ion absolute mobility, μ, can be related to the lithium diffusion coefficient $D = D_0 e^{-\frac{E_m}{k_B T}}$ by the Nernst-Einstein equation:

$$\mu = \frac{D}{k_B T} \tag{1}$$

with T as the temperature in Kelvin, and k_B as the Boltzmann constant. Thus the lithium-ion conductivity can be expressed as:

$$\sigma = \frac{\sigma_o}{T} e^{-\frac{E_A}{k_B T}} \tag{2}$$

Where E_A is the activation energy of diffusion. In the superionic phase, the concentration of mobile species is independent of temperature and E_A can be identified with the energy of migration E_m. An example is α-AgI, stable above 146 °C, where a conductivity of 10^4 higher than for the low-temperature AgI phase can be attributed to the presence of a partially occupied, molten-like cation sublattice.[64] E_A is equal to $E_m+E_f/2$

or $E_m+E_t/2$ for temperature-dependent concentrations of mobile lithium ions in intrinsic and substituted lithium ion conductors, respectively. Plotting the logarithm of the product of conductivity and temperature as a function of the reciprocal of temperature yields apparent activation energy of lithium-ion conduction. Different methods used to measure ion conductivity and diffusion coefficients in solids reported in the literature can be found in the supplementary information. Moreover, the lithium-ion transference number (t_{Li+} which is equal to the ratio of the mobility of lithium ions to the sum of mobilities of all ions), of a crystalline solid can be close to unity.[24] However, the lithium-ion transference numbers of common liquid organic electrolytes are 0.2~0.5,[31,32] making solid-state conductors with ionic conductivities on the order of 2-5 times smaller than aprotic electrolytes equivalently conductive to lithium ions.

Although the lithium-ion conductivity can increase with greater concentrations of mobile lithium ions by aliovalent substitution to create interstitial atoms or vacancies, the conductivity often passes through a maximum and starts to decrease as more mobile species are added into the lattice, where lithium ions are interacting and the mobility of lithium ions is no longer independent.[65] The decrease in the ionic conductivity past the optimum aliovalent substitution can be attributed to increases in the migration energy associated with the local structural distortion induced by the substitution or from passing the optimum concentration of mobile ions and extrinsic defects. Above a critical concentration of substitution, the distortion of the lattice is so strong that the increase in the migration energy or the decrease in extrinsic defects surpasses the effect of increasing the concentration of mobile species and the ionic conductivity decreases. For instance, lithium-ion conductivity in $Li_{3x}La_{2/3-x}\square_{1/3-2x}TiO_3$ perovskites exhibits a dome shape as a function of lithium substitution, x.[21,66] The lithium-ion conductivity becomes greater with increasing lithium concentration for $x \leq 0.12$ (corresponding to an A-site vacancy concentration of ~10%) while a decrease in the conductivity is observed for higher lithium content. Due to the smaller ionic radius of Li^+ (0.92 Å, with a coordination number of 8) compared to La^{3+} (1.36 Å, with a coordination number of 12),[67] the large lithium-ion concentration induces local distortions, which slows down the diffusion and ion conduction. Additionally, the product of the concentration of vacancies and lithium ions reaches a

maximum at x=1/12, if mobility was independent of substitution, one would expect to find a maximum at this value. Similar observations are also noted for lithium-ion conduction in the NASICON structure such as $Li_{1+x}La_xTi_{2-x}(PO_4)_3$[68] and oxygen-ion conduction in the fluorite structure such as $(1-x)ZrO_2$-$(x)Y_2O_3$,[69] as shown in Figure 4. Therefore, the coupling between mobile-ion concentration and lithium-ion mobility or extrinsic defect concentrations highlights challenges in using aliovalent substitution to greatly enhance the conductivity of lithium-ion conductors.

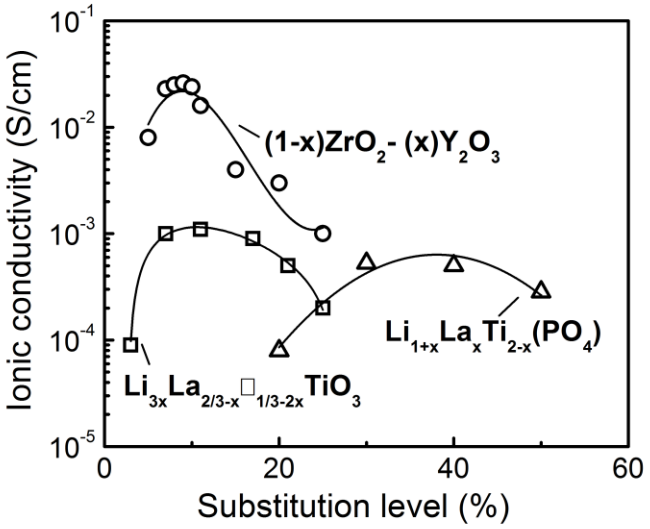

Figure 4. Reported conductivity of lithium ions at room temperature and oxygen ions at 800 ˚C as a function of the substitution concentration, x · 100%, in oxygen conducting $(1-x)ZrO_2$-$(x)Y_2O_3$[69] and lithium conducting $Li_{1+x}La_xTi_{2-x}(PO_4)_3$ NASICON[68] and $Li_{3x}La_{2/3-x}\square_{1/3-2x}TiO_3$ perovskite.[21,66]

3. Enhancing Lithium Conductivity by Structure Tuning

Lithium-ion conductivity has been exploited in a large number of crystal structures and a vast composition space within each family of crystal structures. Room-temperature total lithium-ion conductivity of well-known structures and compositions are shown in Figure 5a. As lithium-ion conductivity measurements are obtained from polycrystalline samples, the presence of grain boundaries

(Figure 6a), which is well known to exhibit greater resistance to ion conduction than the bulk,[70-75] can give rise to reduced conductivity values. For example, the bulk and grain boundary conductivities of LISICON $Li_{2+2x}Zn_{1-x}GeO_4$ (x = 0.55)[72] and perovskite $Li_{0.34}La_{0.51}TiO_3$[49] are shown as a function of temperature in Figure 6b, where the grain boundary conductivities are significantly lower. Controlling the grain boundary contribution to the total ionic conductivity is still a large concern in solid state electrolytes and is still an area that is heavily researched.[76-78] It should be cautioned that reported total conductivities of some ion conductors in Figure 5a may consist of conductivities coming from bulk and grain boundaries.

Two important observations can be made from Figure 5a. First, there are a number of structural families (LISICON-like, argyrodite and garnet) achieving high ionic conductivities in the range of 10^{-2} to 10^{-3} S/cm at room temperature. Of significance to note is that thio-LISCON $Li_{3.25}Ge_{0.25}P_{0.75}S_4$,[79] argyrodite Li_6PS_5Br[80] and garnet $Li_{6.55}La_3Zr_2Ga_{0.15}\square_{0.3}O_{12}$[50] have the maximum conductivity in their structural family while a new class of lithium conductors derived from the thio-LISICON family, $Li_{10}MP_2S_{12}$ (M being Si, Ge, or Sn)[24-26] has shown to have the highest lithium-ion conductivity reported to date. Second, the lithium-ion conductivity within each structural family can vary greatly by up to 5-6 orders of magnitude, which suggests that tuning within a crystal structure can be an effective strategy to enhance ionic conductivity. Although it is not straightforward to find the most conducting compositions by design, and the fastest ion conductors are often found through trial and error,[79] structural tuning by cation substitution within a given structural framework to control bottleneck size for lithium-ion diffusion and lattice volume has been successful in enhancing ionic conductivities, which will be discussed in detail below and structural schematics are provided in the supplementary information.

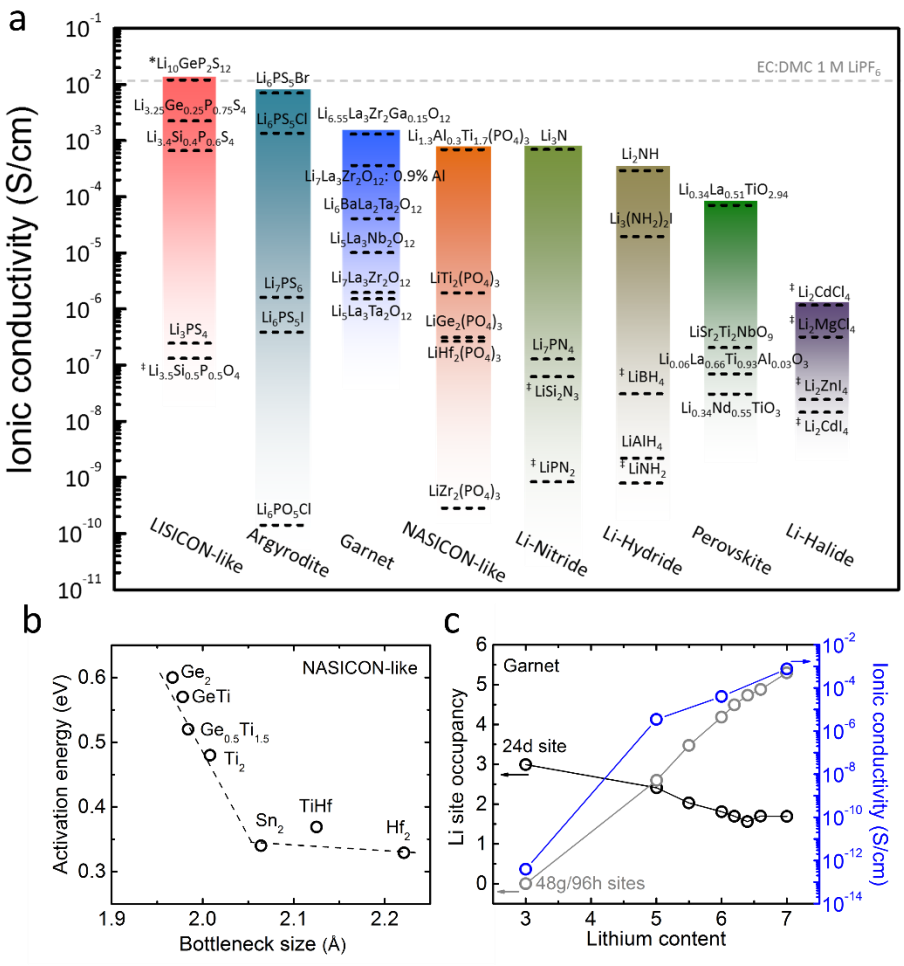

*Figure 5. a) Reported total ionic conductivity of solid-state lithium-ion conductors at room temperature, including LISICON-like (LISICON, thio-LISICON and $Li_{10}GeP_2S_{12}$),[24,79,81-83] argyrodite,[80,84-87] garnet,[50,88-91] NASICON-like,[68,92] Li-nitride,[17,18,93] Li-hydride,[94-97] perovskite[49,98-100] and Li-halide.[101-103]. The lithium-ion conductivity of EC:DMC 1 M $LiPF_6$ is shown for comparison as a dashed gray line.[27] *$Li_{10}GeP_2S_{12}$ is placed in the LISCON-like structural family for its chemical and structural similarity to the other compounds. ‡Compounds whose conductivity have been extrapolated from higher temperatures to room temperature (see Table S1 for details of values used for extrapolation). b) Activation energy derived from bulk conductivity as a function of bottleneck size between M1 and M2 sites (see Figure 3d in the supplementary information for the positions of these sites in the NASICON-like structure) as estimated from simulated structures for the compositions $LiGe_2(PO_4)_3$ (Ge_2), $LiGeTi(PO_4)_3$ (GeTi), $LiGe_{0.5}Ti_{1.5}(PO_4)_3$ ($Ge_{0.5}Ti_{1.5}$),*

$LiTi_2(PO_4)_3$ (Ti_2), $LiSn_2(PO_4)_3$ (Sn_2), $LiTiHf(PO_4)_3$ (TiHf), and $LiHf_2(PO_4)_3$ (Hf_2) from Martinez-Juarez et al.[16] The dashed lines are guides to the eye. c) Ionic conductivity (blue) for $Li_3Tb_3Te_2O_{12}$ (extrapolated), $Li_5La_3Ta_2O_{12}$, $Li_6BaLa_2Ta_2O_{12}$ and $Li_7La_3Zr_2O_{12}$ and lithium site distribution in the 48g/96h octahedral positions (gray) and 24d tetrahedral positions (black) from Thangadurai et al.[15]

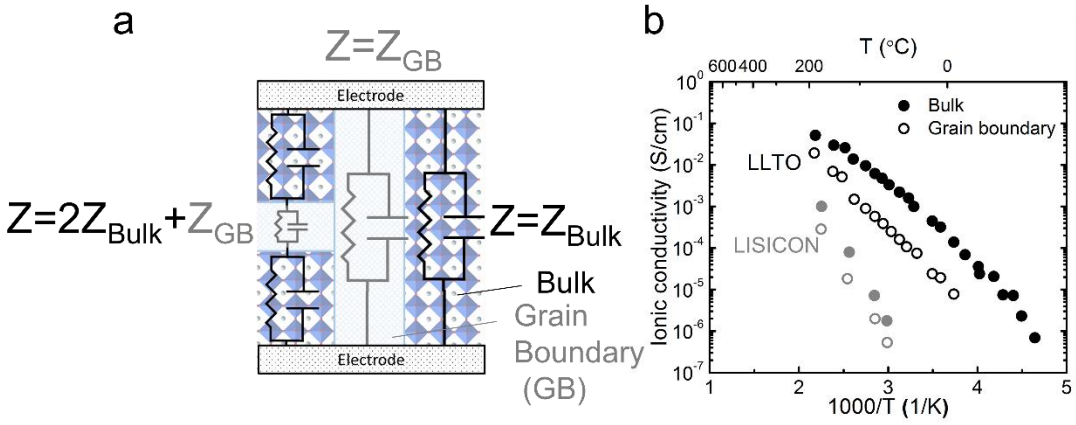

Figure 6. a) Schematic of conduction pathways in polycrystalline material (path on the left and middle where ions must move through the bulk and grain boundary regions or only through the grain boundaries, respectively) and layered single-crystal films (path in the middle and on the right where ions can move parallel to the layers of material. This case is rarely found in application). b) Separated bulk and grain boundary conductivities as a function of temperature for LLTO: $Li_{0.34}La_{0.51}TiO_{2.94}$[49] and LISICON: $Li_{2+2x}Zn_{1-x}GeO_4$ ($x = 0.55$).[72]

3.1. LISICON-like

The LISICON and thio-LISICON compounds crystallize into structures similar to the γ-Li_3PO_4 structure with an orthorhombic unit cell and *Pnma* space group (space group number 62. All space group numbers are from the International Union of Crystallography),[104] where all cations are tetrahedrally coordinated.[105] The structure can be thought of as a distorted hexagonal close-packing of oxygen atoms whose packing planes are perpendicular to the c-axis and in which cations (for instance lithium and phosphorus as in Li_3PO_4) are distributed in two crystallographically distinct tetrahedral interstices, forming parallel one-dimensional chains along the a-axis. The lithium ions which are located in LiO_4 tetrahedra

diffuse between these tetrahedra and interstitial sites located in the PO_4 network.[106] Aliovalent substitution of P^{5+} by Si^{4+} or Ge^{4+} in γ-Li_3PO_4 can create compositions such as $Li_{3+x}(P_{1-x}Si_x)O_4$,[107-109] which give rise to fast lithium-ion conduction and the LISICON family. The excess lithium ions created by this substitution, which cannot be accommodated in the tetrahedral sites of the structure, occupy interstitial sites, making the adjacent lithium-lithium ion distance unusually short and resulting in a high conductivity of 3 x 10^{-6} S/cm, as shown in Figure 5. Substituting O by S in $Li_{3+x}(P_{1-x}Si_x)O_4$ to form $Li_{3+x}(P_{1-x}Si_x)S_4$, giving rise to the thio-LISICON family, can further increase lithium-ion conductivity by three orders of magnitude at room temperature[82] (ionic conductivity of 6 x 10^{-4} S/cm in Figure 5a).

The $Li_{10}MP_2S_{12}$ (M = Si, Ge or Sn) [24-26] and $Li_{11}Si_2PS_{12}$[110] family has the highest lithium ion conductivities above 10^{-2} S/cm at room temperature. The $Li_{10}GeP_2S_{12}$ (LGPS) structure has the space group *$P4_2/nmc$* (space group number 137) with a tetragonal unit cell made of isolated PS_4 and GeS_4 tetrahedra, which occupy two distinct crystallographic sites: the 2b sites that are fully occupied by phosphorus and the 4d sites that are partially shared by germanium and phosphorus at the ratio 1:1. Lithium atoms are distributed over 4 crystallographic sites (4c, 4d, 8f and 16h). The octahedrally coordinated lithium (4d sites) is edge shared with 4d (P/Ge)S_4 tetrahedra along the c-axis and corner shared with 2b PS_4 tetrahedra along the a- and b-axis, forming the backbone of the structure. The lithium atoms in these 4d octahedral sites are believed to be less mobile that those in the two other tetrahedrally coordinated sites (the 8f and 16h sites) which form one-dimensional chains of edge-sharing tetrahedra.[24,25,111,112] The calculated energy of migration through the one-dimensional channel is low (0.17 eV) whereas the diffusion in the *ab* plane is larger (0.28 eV), owing to relatively less mobile lithium ions in the LiS_6 octahedra bridging the channels of diffusion[113]. However, recent computational works suggests that the lithium diffusion in LGPS might be possible in the *ab* plane in addition to the diffusion into the channels along the c-direction,[112,113] which is made possible by the connection of the one-dimensional chains of diffusion through a position previously neglected (4c sites).[111] Having an optimum channel size for lithium-ion migration is critical to achieve high lithium-ion conductivity. The tin-based compound $Li_{10}SnP_2S_{12}$ [25] has a larger unit cell due the larger size of tin than germanium, but shows a lower ionic conductivity (4 mS/cm at 300 K, compared to 12 mS/cm at

300 K for LGPS). While the volume of the unit cell increases steadily as one goes from Si to Ge to Sn, the solid solutions $Li_{10}(Ge_{1-x}M_x)P_2S_{12}$ (M = Si, Sn) with $0 \leq x \leq 1$ for Sn and $0 \leq x < 1$ for Si[114] exhibit a conductivity maximum at the composition $Li_{10}Ge_{0.95}Si_{0.05}P_2S_{12}$ reaching 8.6 mS/cm, which has the optimum tunnel size close to LGPS, as supported by *ab-initio* molecular dynamics.[115] Both $Li_{3.25}Ge_{0.25}$ $P_{0.75}S_4$ and $Li_{10}GeP_2S_{12}$ were experimentally shown to have a wide electrochemical stability window with no electrochemical reactions between 0 – 4 V versus Li/Li^+.[24,79] However, computational results have in some cases concluded $Li_{10}GeP_2S_{12}$ is stable in some cases[116] and unstable in others.[113,115] When in contact with lithium $Li_{10}GeP_2S_{12}$ from computational studies has been found to be unstable.[113,115]

3.2. Argyrodite

Lithium argyrodite Li_6PS_5X (with X = Cl, Br or I) are newly discovered fast lithium-ion conductors (the ionic conductivities approach as high as 7×10^{-3} S/cm as reported by Deiseroth et al.[14]) isostructural to the Cu- and Ag-argyrodite compounds which crystallize into a structure based on tetrahedral close packing of anions (cubic unit cell with space group $F\bar{4}3m$, space group number 216).[14,80,84-86,117,118] Within this close packed structure, phosphorus atoms fill tetrahedral interstices, forming a network of isolated PS_4 tetrahedron (similarly to the thio-LISICON structure), while lithium ions are randomly distributed over the remaining tetrahedral interstices (48h and 24g sites). Lithium-ion diffusion occurs through these partially occupied positions forming hexagonal cages, which are connected to each other by an interstitial site around the halide ions in the case of Li_6PS_5Cl and around the sulfur anions in Li_6PS_5I[80]. The activation energy is rather low, in the range from 0.2 to 0.3 eV, owing to facile diffusion in between the hexagons made of partially occupied positions.[119] The difference in the connectivity of the hexagonal cages and the distribution of lithium among the different sites as well as the disorder on the S^{2-}/X^- sublattice which exist in chloride and bromide, but not in iodide, may explain why Li_6PS_5I has significantly lower ionic conductivity compare to Li_6PS_5Cl and Li_6PS_5Br (Figure 5a). This variation in ionic conductivity highlights the importance of disorder in promoting high ionic conductivity.[119] It is also important to note that the substitution of sulfur by oxygen leads to a decrease by several order of magnitudes in conductivity, a trend

similar to what is found in LISICON and thio-LISICON conductors. Preliminary tests show that the electrochemical stability window of Li_6PS_5X (X=Cl, Br, I) argyrodite compounds are very wide (0 -7 V versus Li/Li^+).[84]

3.3. NASICON-like

The NASICON framework, generally with a rhombohedral unit cell and space group $R\bar{3}c$ although monoclinic and orthorhombic phases have been reported,[92,120] of $L_{1+x}M^{4+}_{2-x}M'^{3+}_x(PO_4)_3$ phosphates (L = Li or Na and M = Ti, Ge, Sn, Hf or Zr and M' = Cr, Al, Ga, Sc, Y, In or La) consists of isolated MO_6 octahedra interconnected via corner sharing with PO_4 tetrahedra in alternating sequences.[68,120-124] Lithium can occupy two different sites in the structure: the M1 sites that are 6-fold coordinated (octahehedral symmetry) located directly between two MO_6 octahedra, and the M2 sites that are 8-fold coordinated and located between two columns of MO_6 octahedra. Lithium migration occurs via hopping between these two sites, and partial occupancies of lithium ions on those two sites is crucial for fast lithium-ion conduction, especially as vacancies are required at the intersection of the conduction pathways to give access to three-dimensional diffusion within the structure.[125-127] We summarize two strategies reported to increase lithium-ion conductivity. First, changing the size of the network can greatly influence lithium-ion conductivity, where the bottleneck of lithium-ion conduction often resides in the migration between these two sites. For example, making the bottleneck size larger by using greater M ion sizes in $LiMM'(PO_4)_3$ from M/M' = Ge^{4+} (0.53 Å), Ti^{4+} (0.605 Å) to Hf^{4+} (0.71 Å) can increase lithium-ion conductivity up to four orders of magnitude[16], as shown in Figure 5a. Of significance to note, the activation energy of lithium-ion conduction for these $LiMM'(PO_4)_3$ decreases linearly with the bottleneck size between the M1 and M2 sites,[16] which further supports optimizing bottleneck sizes for mobile ions being critical to generate fast ion conduction, as shown in Figure 5b. Second, aliovalent substitution[68] by M'^{3+} cations such as Al^{3+} and Sc^{3+} in $LiMM'(PO_4)_3$ can greatly increase the conductivity by increasing the mobile lithium concentration and mobility. However, the substitution level is limited to ~15% (x = 0.3) due to the large ionic radius mismatch, above this level the formation of a secondary phase is observed for Al^{3+} or Sc^{3+} for instance.[68]

$Li_{1.3}Al_{0.3}Ti_{1.7}(PO_4)_3$ has the highest bulk conductivity ($\sigma \approx 3 \times 10^{-3}$ S/cm) for NASICON lithium-ion conductors at room temperature reported to date.[68] Additionally, NASICON-like conductors are typically stable with air and water, and are stable at high potentials.[128] However, similar to perovskites, titanium containing compounds can be reduced at low potentials.[45,128,129]

3.4. Garnet

These oxides are derived from the ideal garnet structure with the general formula $A_3B_2(XO_4)_3$ such as $Ca_3Al_2(SiO_4)_3$ (cubic unit cell and space group $Ia\bar{3}d$, space group number 230). A-sites are 8-fold coordinated (antiprismatic sites), B-sites are 6-fold coordinated (octahedral sites) and X-sites are 4-fold coordinated (tetrahedral sites). In lithium-conducting garnets, lithium ions occupy the tetrahedral positions as in $Li_3Nd_3Te_2O_{12}$. However, to obtain appreciable ionic conductivity at room temperature, more lithium can be added into the structure by adjusting the valence of the A and B cations leading to several stoichiometries of lithium-conducting garnets such as $Li_3Ln_3Te_2O_{12}$ (Ln = Y, Pr, Nd, Sm-Lu), $Li_5La_3M_2O_{12}$ (M = Nb, Ta, Sb), $Li_6ALa_2M_2O_{12}$ (A = Mg, Ca, Sr, Ba; M = Nb, Ta) and $Li_7La_3M_2O_{12}$ (M = Zr, Sn).[15] $Li_3Ln_3Te_2O_{12}$ garnets, where lithium ions reside only in the tetrahedral sites, have low ionic conductivities.[130,131] In addition, introducing M^{5+} ions in the garnet structure introduces extra lithium ions in $Li_5La_3M_2O_{12}$, which are distributed over tetrahedral (24d sites) and distorted octahedral sites (48g/96h sites). Moreover, replacing La^{3+} with divalent ions and M with Zr^{4+} in $Li_5La_3M_2O_{12}$ leads to greater lithium-ion concentrations in $Li_6ALa_2M_2O_{12}$ and $Li_7La_3M_2O_{12}$. Generally speaking, increasing the lithium-ion concentration in the garnet structure renders faster lithium-ion conduction.[132] However, the aliovalent substitution of La by Ba increases the conductivity, where the extent of increase cannot be explained by the increase of lithium concentration.[89,133,134] For example, an order of magnitude increase in the ionic conductivity is noted going from $Li_5La_3Ta_2O_{12}$ to $Li_6BaLa_2Ta_2O_{12}$ as shown in Figure 5a. The aliovalent substitution can induce changes in the lithium-ion distribution in the tetrahedral and octahedral sites.[135,136] Having lithium ions occupy the distorted octahedral sites is crucial to increase the total ionic conductivities by nine orders of magnitude from $Li_3Ln_3Te_2O_{12}$ to $Li_7La_3M_2O_{12}$, as shown in Figure 5c.[15] Moreover, the

aliovalent substitution of Zr by Sb (20%),[137] Ta (50%)[138] or Nb (100%) can significantly improve the conductivity of $Li_7La_3Zr_2O_{12}$ (LLZO) through modification of the lithium distribution, as in the case of Sb, or through the increase in lithium concentration, as in the case of Ta. The effect of aliovalent substitution is shown in Figure 5 and 7 with the increase in conductivity through substitution of Zr by Nb in $Li_5La_3Nb_2O_{12}$.[90] Having the cubic structure for LLZO is also critical to achieve high ionic conductivity, where lithium ions are disordered on the tetrahedral and octahedral sites. Aluminum doping (0.9 wt%) stabilizing LLZO in the cubic form, enhances the lithium-ion conductivity by two orders of magnitude and lowers the activation energy (0.34 eV for Al-doped garnet vs. 0.49 eV for undoped) relative to the tetragonal undoped $Li_7La_3Zr_2O_{12}$, where lithium ions are ordered on tetrahedral and octahedral sites,[139,140] as shown in Figure 5a.[88] Furthermore, the formation of $LiAlSiO_4$ and $LiGaO_2$ at the grain boundaries can also contribute to the high conductivity of the Al-doped LLZO[141] and Ga-substituted LLZO.[142] Further, these garnet lithium electrolytes have been found to have high thermal stabilities up to 900 °C and to be stable against lithium metal,[143] although some reports of instabilities against positive electrodes has been shown.[15,144]

3.5. Perovskite

The ideal perovskite structure with a general formula ABO_3, cubic unit cell, and space group $Pm\bar{3}m$ (space group number 221) consists of A-site ions (typically alkaline-earth or rare-earth elements) at the corners of a cube, B ions (typically transition metal ions) at the center and oxygen atoms at the face-center positions, where A sites are in 12-fold coordination and B sites are in 6-fold coordination (BO_6) that share corners with each other. Lithium can be introduced in the perovskite on the A site through aliovalent doping creating compositions such as $Li_{3x}La_{2/3-x}\square_{1/3-2x}TiO_3$. Introduction of lithium modifies both the concentration of lithium and vacancies, and the concentration of vacancies and their interactions[145] (that can lead to ordering of lithium/vacancies in the planes perpendicular to the c axis) can significantly influence ionic conductivity. Lithium ions can diffuse by jumping in the *ab* plane to an adjacent vacancy through a square planar bottleneck made of oxygen forming the corners of the octahedra at room temperature.[20,21] A recent computational study suggests that in the case where there is not significant

ordering of the A-site cations in layers normal to the c-axis, lithium ions could also diffuse along c-axis, which is in better agreement with experimental conductivity results.[146] The bottleneck size can be increased by using large rare earth or alkaline earth metal ions in the A site, which can lead to significant increases in the ionic conductivity. A systematic increase in the bulk ionic conductivity at 400 K and lowered activation energy correlates with increasing rare earth metal ion size ($Sm^{3+} < Nd^{3+} < Pr^{3+} < La^{3+}$).[12,100] For example, replacing Nd^{3+} with La^{3+} in $Li_{0.34}M_{0.55}TiO_3$ increases the ionic conductivity by four orders of magnitude at room temperature, as shown in Figure 5. The highest lithium-ion conductivity in the perovskite family was found for $Li_{0.34}La_{0.56}TiO_3$ with a total lithium-ion conductivity of 7×10^{-5} S/cm and bulk ionic conductivity of 10^{-3} S/cm. In addition to the tuning of the bottleneck size, changing the bond strength between the B-site cation and the oxygen has been suggested to influence the conductivity. However, this effect has been reported for a narrow concentration range of Ti^{4+} substitution by Al^{3+},[147] which results in an increased conductivity. While lithium lanthanum titanates have been shown to be stable at high potentials, it is known to be reduced around 1.5 V versus Li/Li^+ making it unsuitable for use with lithium and graphite negative electrodes.[20,148]

3.6. Relating Lattice Volume to Lithium-Ion Conductivity

Tuning lattice volume by substitution

Increasing the lattice volume can increase the lithium-ion conductivity and reduce the activation energy for several structural families. By comparing the lithium-ion conductivity with isovalent substitution, increasing the lattice volume per lithium atom within a given crystal structure leads to increased ionic conductivity and lowered activation energy for LISICON-like $Li_{3.5}M_{0.5}M'_{0.5}O_4$ [13,108,149,150] (Figure 7a), NASICON-like $LiM_xM'_{2-x}(PO_4)_3$[16,151] (Figure 7b), and perovksite $Li_{3x}M_{2/3-x}\square_{1/3-2x}TiO_3$[100] (Figure 7c). Of significance to note is that increasing lattice volume per lithium atom in NASICON $LiM_xM'_{2-x}(PO_4)_3$ in Figure 7b correlates with larger bottleneck size for lithium ion diffusion (Figure 5b and Figure S3). Moreover, increasing lattice volume with larger A site rare earth metal ions (Sm < Nd < Pr <

La) in the perovskite structure has been correlated with increased lithium-ion conductivity and reduced activation energy.[100]

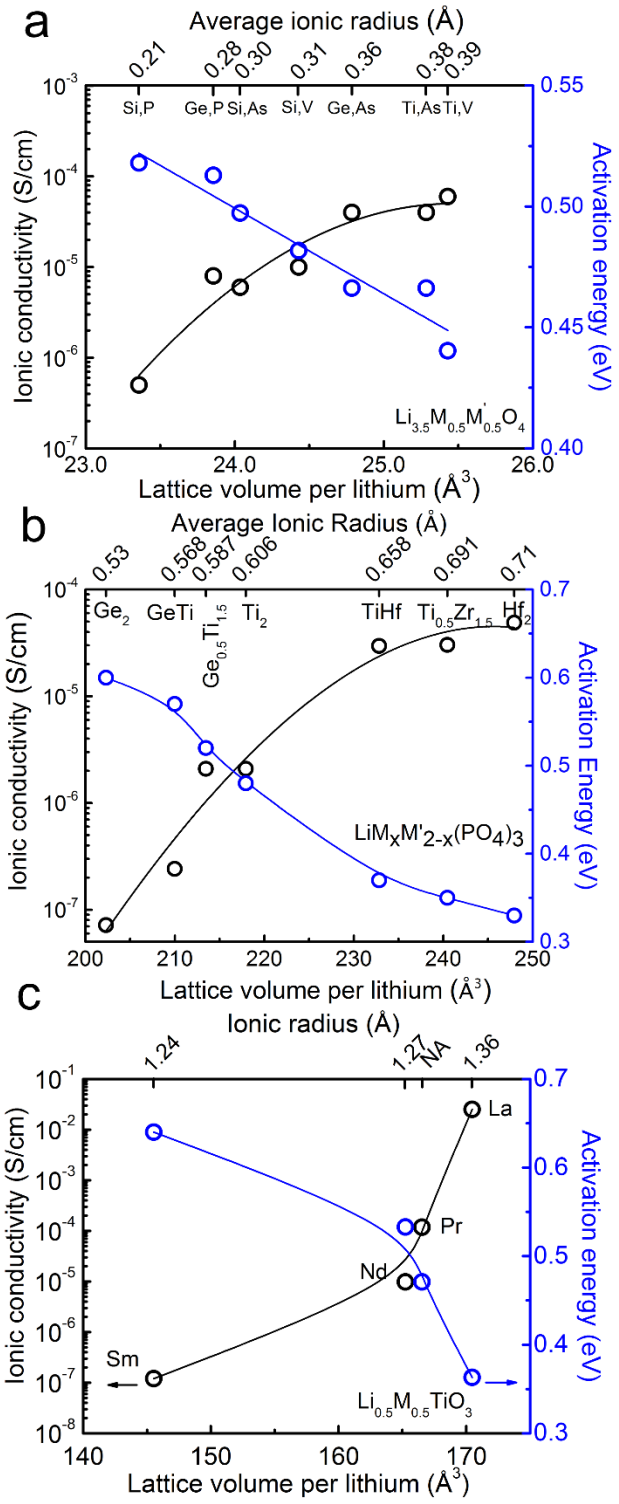

Figure 7. a) and b) Lithium-ion conductivity of LISICON $Li_{3.5}M_{0.5}M'_{0.5}O_4$ and NASICON $LiM_xM'_{1-x}(PO_4)_3$ with different cationic radii at room temperature (adapted from references [13,108,149,150] for LISICON and references [16,151] for NASICON) as a function of lattice volume per lithium atom. c) Ionic conductivity at 400 K and activation energy as a function of lattice volume per lithium atom for perovskites $Li_{0.5}M_{0.5}TiO_3$ with A-site rare earth metal ions M=Sm, Nd, Pr, and La adapted from Itoh et al.[100] The average ionic radius was calculated using Shannon's radii, Pr^{3+} in 12 fold coordination is not available and is shown as NA.[67]

Tuning lattice volume by mechanical Strain

Changing lattice volume can be also exploited by imposing tensile or compressive strains in ion conductors.[152-155] DFT studies on cubic $Li_7La_3Zr_2O_{12}$ (c-LLZO),[138] and LGPS [115] (Figure 8a) show that isotropic compressive strain can greatly decrease lithium-ion conductivity while tensile strain does not lead to any significant enhancement in the ionic conductivity, suggesting that the lattice volume per formula unit of these two conductors is near optimal or further increasing lattice volume does not greatly reduce the activation energy of lithium ions passing through bottleneck points in the structure. Experimental validation of strain-tailored lithium-ion conductivity is scarce, which can be attributed to the difficulty to make epitaxial thin films due to high vapor pressure of lithium[156] and the growth of secondary phases during the deposition.[157] Recent advances in thin-film growth of lithium-ion conductors[158-160] suggest that it is possible to tailor lithium-conductivity by strains imposed by lattice mismatch relative to the substrate. For example, epitaxial $Li_{0.33}La_{0.56}TiO_3$ thin films grown on $NdGaO_3$ (NGO) show an anisotropy of ionic conductivity along the a and b axes of $Li_{0.33}La_{0.56}TiO_3$, which may result from different strains imposed by NGO along these two crystallographic directions.[161] However, due to the small variation in the measured ionic conductivity, further studies are needed in order to firmly establish the influence of strain on Lithium conductivity.

More compelling examples of ionic-conductivity tuning using strains can be found ion oxygen-ion-conducting thin films.[162-164] For example, the migration energy for oxygen-ion diffusion in stabilized zirconia (YSZ) thin films of 1 nm in thickness significantly decreases with increasing tensile strains

imposed from Al_2O_3 to $KTaO_3$ substrate, as shown in Figure 8b.[164] This trend is supported by experimentally measured activation energies of oxygen-ion conductivity of YSZ thin films shown in Figure 8c, where negative strain imposed by Sc_2O_3 [165] increases the activation energy while tensile strain imposed by Y_2O_3 [163] or Al_2O_3 [166]decreases the activation energy. As the tensile strain is increased the activation energy is decreased, as is found for YSZ/Al_2O_3 and YSZ/Y_2O_3 with a lower nominal strain of 4 and 3%, respectively.[162,163,167] As the strains imposed from the substrate reduces with increasing film thickness, the observed changes in the activation energy decrease with increasing thickness, as shown in Figure 8c. The lowest activation energy is observed for the thinnest YSZ film of 6 nm on Al_2O_3, translating to an increase in the conductivity of 1.5 order of magnitude at 300 °C.[166] Caution should be taken when assessing ion-conductivity changes of these thin-film studies. First, thin films grown on different substrates can greatly vary from study to study. For example, no change is observed for oxygen-ion conductivity for YSZ thin films (30-300 nm) grown on MgO, Al_2O_3 or $SrTiO_3$[168] single-crystal substrate and YSZ/CeO_2 multilayers.[169] Second, other factors besides strain, such as changes in the nature of metal-oxygen bonds between oxygen sub-lattices at the interface,[170] mobile ion concentration[171] and new phases[170] created at the interface should also be considered.

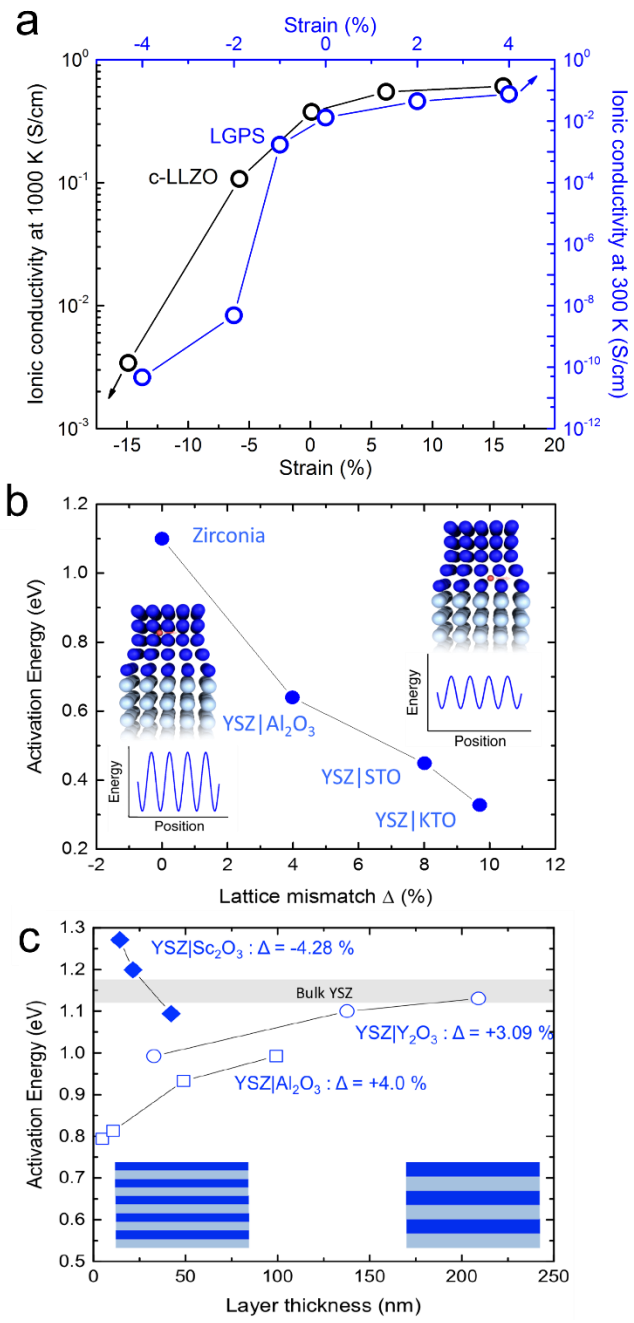

Figure 8. a) Variation of computed ionic conductivities in LGPS[115] and cubic LLZO[138] as a function of applied isotropic strain. The ionic conductivity decreases dramatically under applied compressive strain while only a relatively moderate improvement is obtained under tensile strain. b) *Activation energy of YSZ as a function of lattice mismatch computed from ab-initio molecular dynamics (AIMD).[164] The structure used in the calculation was 1 nm of YSZ sandwiched between different substrates ($KTaO_3$ (KTO), Al_2O_3,*

and $SrTiO_3$ (STO)). c) Activation energy of YSZ on different substrates measured experimentally as a function of film thickness: Y_2O_3/YSZ multilayers,[163] Sc_2O_3/YSZ multilayers[165] and Al_2O_3/YSZ thin films.[166] The horizontal gray bar represents the activation energy of bulk YSZ. As the interfaces between layers are semi-coherent, the lattice mismatch Δ cannot be directly identified as the lattice strain.

3.7. COMPARISON OF NORMALIZED LITHIUM ION CONDUCTIVITY

Here we compare the normalized ionic conductivity and activation energy of lithium-ion conduction among selected structural families (Figure 9). The ionic conductivities were normalized by dividing the ionic conductivity by $(\frac{cq^2}{k_BT})$ resulting in the so called normalized ion conductivity, with k_B being the Boltzmann constant, *T* being temperature, *c* being the concentration of lithium, and *q* being the charge of each lithium ion, which are shown in Table 1 and Figure 9. The lithium concentration was calculated using the formula $c = \frac{NZ}{V}$ with N being the number of lithium per formula unit (for ex. N=3 in Li_3PO_4), V is the volume of the unit cell in cm^3 and Z is the number of formula units per unit cell (for ex. Z=4 for Li_3PO_4 because the unit cell contains 12 lithium atoms). This quantity deviates from the diffusion coefficient as not all of the lithium in the formula unit are necessarily mobile, and thus the normalized ionic conductivities reported are the lower bound for the diffusion coefficients, providing some insights into lithium mobility of the mobile species in a given structure. It should also be noted that the Haven ratio (ratio of self-diffusion to charge diffusion. The charge diffusion is the diffusion coefficient calculated through measurements of the ionic conductivity.) would also need to be taken into account, although this value is typically on the order of unity. Although we use bulk conductivities for ion conductors when available (NASICON-like and perovskite families), it should be cautioned that reported conductivities of some ion conductors may consist of conductivities coming from bulk and interfacial or grain boundaries (LISICON-like and garnet families).

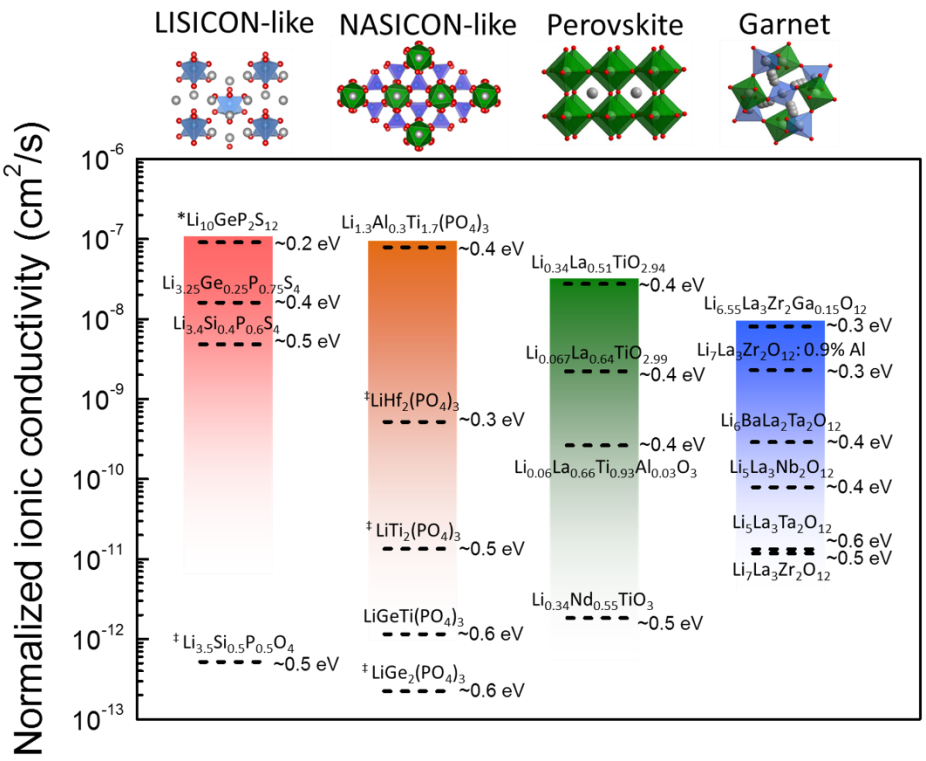

*Figure 9. Normalized ionic conductivities and activation energies at room temperature and structures for select lithium-ion conductors. The values are taken from literature for LISICON-like and $Li_{10}GeP_2S_{12}$,[24,79,82,83] NASICON-like,[16,68] perovskite[49,98,100,172] and garnet[50,88-91,139,173]. See Table 1 for details of the normalization of the ionic conductivity. The bulk conductivity of the perovskite and NASICON-like conductors are used as they are available in the literature while the total conductivities are used for LISICON-like and garnet conductors. In the structure schematics, gray balls represent lithium ions and red balls represent oxygen ions. For more detailed schematics see supplementary information. *$Li_{10}GeP_2S_{12}$ is placed in the LISCON-like family for its chemical and structural similarity to the other compounds. ‡Compounds whose conductivity have been extrapolated from higher temperatures to room temperature (see Table S1 for details of values used for extrapolation).*

*Table 1. Calculations of normalized ionic conductivities shown in Figure 9. *$Li_{10}GeP_2S_{12}$ is placed in the LISCON-like family for its chemical and structural similarity to the other compounds. ‡Compounds which have been extrapolated from higher temperatures to room temperature (see Table S1 for details of values used for extrapolation).*

		Ionic conductivity (S/cm)	Lattice parameters a b c (Å)			Lattice Volume ($Å^3$)	Z	Temperature (K)	Normalized ionic conductivity (cm^2/s)	Reference
LISICON-like	*$Li_{10}GeP_2S_{12}$	1.20E-02	8.69	8.69	12.60	952.35	2	300	9.25E-08	Kamaya et al. 2011[24]
	$Li_{3.25}Ge_{0.25}P_{0.75}S_4$	2.20E-03	13.40	7.66	6.07	621.75	4	298	1.69E-08	Kanno et al. 2001[79]
	$Li_{3.4}Si_{0.4}P_{0.6}S_4$	6.40E-04	13.37	7.88	6.11	643.50	4	300	4.90E-09	Murayama et al. 2002[82]
	‡$Li_{3.5}Si_{0.5}P_{0.5}O_4$	1.31E-07	10.60	6.12	5.01	324.83	4	300	5.06E-13	Deng et al. 2015[83]
NASICON-like	$Li_{1.3}Al_{0.3}Ti_{1.7}(PO_4)_3$	3.00E-03	8.50	8.50	20.82	1302.71	6	298	8.05E-08	Aono et al. 1990[68]
	‡$LiHf_2(PO_4)_3$	1.29E-05	8.83	8.83	22.03	1487.53	6	300	5.17E-10	Martinez-Juarez et al. 1998[16]
	‡$LiTi_2(PO_4)_3$	3.83E-07	8.51	8.51	20.85	1307.54	6	300	1.35E-11	Martinez-Juarez et al. 1998[16]
	$LiGeTi(PO_4)_3$	3.48E-08	8.41	8.41	20.58	1259.86	6	300	1.18E-12	Martinez-Juarez et al. 1998[16]

	‡$LiGe_2(PO_4)_3$	6.62E-09	8.28	8.28	20.47	1213.90	6	300	2.17E-13	Martinez-Juarez et al. 1998[16]
Perovskite	$Li_{0.34}La_{0.51}TiO_{2.94}$	1.00E-03	3.87	3.87	3.87	58.01	1	300	2.76E-08	Inaguma et al. 1993[49]
	$Li_{0.067}La_{0.64}TiO_{2.99}$	7.90E-05	3.87	3.88	3.89	58.41	1	300	2.20E-09	Inaguma et al. 1994[172]
	$Li_{0.06}La_{0.66}Ti_{0.93}Al_{0.06}O_3$	1.68E-06	3.87	3.87	3.89	58.33	1	300	2.65E-10	Morata-Orrantia et al. 2002[98]
	$Li_{0.34}Nd_{0.55}TiO_3$	7.00E-08	3.83	3.83	3.83	56.05	1	300	1.87E-12	Itoh et al. 1994[100]
Garnet	$Li_{6.55}La_3Zr_2Ga_{0.15}\square_{0.3}O_{12}$	1.30E-03	12.98	12.98	12.98	2187.38	8	297	8.13E-09	Bernuy-Lopez et al. 2014[50] and Rettenwander et al. 2014[173]
	$Li_7La_3Zr_2O_{12}$: 0.9% Al	3.55E-04	12.97	12.97	12.97	2183.19	8	300	2.24E-09	Buschmann et al. 2011[88]
	$Li_6BaLa_2Ta_2O_{12}$	4.00E-05	12.95	12.95	12.95	2169.74	8	295	2.88E-10	Thangadurai et al. 2005[89]
	$Li_5La_3Nb_2O_{12}$	1.00E-05	12.81	12.81	12.81	2099.61	8	295	8.35E-11	Peng et al. 2013[90]
	$Li_7La_3Zr_2O_{12}$	2.00E-06	13.13	13.13	12.66	2184.39	8	300	1.26E-11	Buschmann et al. 2011[88] and Awaka et al. 2009[139]
	$Li_5La_3Ta_2O_{12}$	1.54E-06	12.85	12.85	12.85	2121.82	8	298	1.31E-11	Gao et al. 2010[91]

After normalizing the ionic conductivity, one can note that the differences among conductors within a family is not significantly altered, which results from the concentration of lithium ions within each family not significantly changing (although we are unable to take into account the change in the true mobile charge carriers between compounds). However, after normalization, the difference between the LISICON-like family and the NASICON-like and perovskite families significantly decreases and the difference between the garnet family increases. As the concentration of lithium is higher in LISICON-like than NASICON-like and perovskites families, after normalization the difference decreases. This suggests that the mobility of lithium ions in the NASICON-like and perovskite families is not significantly different from the LISICON-like family. With a similar argument, one can note that the garnet family falls below all the others, which indicates that, in general, the garnet family has a very high concentration of lithium, but the lithium-ions are less mobile compared to the other families. In addition, assuming that close to all the lithium are mobile in the compounds with the highest conductivity within LISICON-like, NASICON-like, and perovskite families, the approximate diffusion coefficient for the best conductor in each family all approach 10^{-7} cm/s^2.

When comparing the different families of solid state electrolytes some general trends can be found. The LISICON-like and LMPS electrolytes typically have very high conductivities, but only when sulfur is used as the anion within the structure. These sulfides have the drawback that they are water sensitive and must be handled under an inert atmosphere and also are in general less stable.[128] Additionally, the high volatility of sulfur compounds makes the stoichiometry harder to control when synthesizing these compounds. Similar complications are to be expected for the sulfide argyrodite conductors, which also require handling to be done in inert environments.[80] However, both the LISICON-like and argyrodite families, with their high conductivities, are sure to remain heavily-researched structures for lithium solid-state electrolytes. The perovskites have lower total conductivities (that from bulk and grain boundaries) than other families. Additionally, the perovskite materials require high-temperature sintering where Li_2O loss can be an issue and they have a decreased stability against lithium metal as Ti^{4+} cations are easily

reduced when in contact with lithium metal.[45,148] Similar problems with NASICON-like compounds are found as the Ti^{4+} cations can be reduced.[45,128,129] The NASICON-like materials also are in general less conductive than the LISICON-like and garnet materials. Garnet solid state electrolytes are a promising class of conductors that do not seem suffer from some of the hindrances of the other conductors such as chemical instability or synthesis concerns, although recent reports do suggest that careful attention must be paid to sintering conditions, including the sintering atmosphere, in order to achieve high densities and conductivities.[15,174]

4. Reported Descriptors of Ionic Conductivity

Fundamental understanding of physical parameters governing lithium-ion conductivity among different families of crystal structures is critical to design new solid-state electrolytes with enhanced conductivity and stability. Here we seek and discuss some of physical parameters that can be drawn to rationalize ionic conductivity trends among different crystal structures.

4.1. Volume of Diffusion Pathway

The volume accessible to lithium in the structure might be used a descriptor for lithium-ion conductivity among different structural families. In the previous section, we show that the ionic conductivity and activation energy correlates with the lattice volume and/or bottleneck sizes within a given structure (Figure 5 and Figure 7). Adam and Swenson proposed a new method to determine the diffusion pathway using the bond valence method.[175] The main concept in the bond valence method is the notion of the 'valence' of a chemical bond between the atom i and j, s_{i-j}, which can be calculated using the formula:

$$s_{i-j} = \exp\left[\frac{R_o - R}{b}\right] \qquad (3)$$

where R is the bond length and R_o and b can be considered, to a good approximation, as constants that don't depend on the crystal structure being considered. It has been found empirically[176] that if a crystal is stable, the bond valence sum of each atom $i, V_i = \sum_j s_{i-j}$, where j runs over all nearest neighbors, will be

very close to the formal charge of that atom. To determine the diffusion pathway, the unit cell is divided into a fine 3D grid. At each node of this grid, the bond valence sum of the diffusing species is calculated. The diffusion pathway in crystalline and amorphous solids corresponds to a percolating region, where the bond valence mismatch of the mobile species, defined as the difference between the bond valence sum and the formal charge, is below a certain threshold.[175]

The value of this threshold can significantly influence the volume and the topology of the diffusion pathway in a given structure. If the threshold is too small then there will be no percolating diffusion pathway but only disconnected regions as can be seen in magenta in Figure 10a in the case of Li_6PS_5Cl. On the contrary, if the threshold is too large, then the entire unit cell will become part of the diffusion pathway, a situation obviously non-physical. Unfortunately, there is no unique way to determine the value of this critical parameter. One possibility is to choose the lowest value of the bond valence mismatch at which a percolating pathway starts to appear (which is shown in cyan in Figure 10a). A fixed value of the bond valence mismatch of 0.2 has also been used to determine the diffusion pathway in Li^+, Na^+, K^+, Ag^+ and Cu^+ conductors.[177]

The ionic conductivity as well as the activation energy of diffusion in silver-, sodium-, and lithium-ion-conducting glasses correlate linearly with the product of the fractional volume of diffusion pathway (F), defined as the ratio between the volume of diffusion pathway and the volume of the unit cell, and the square root of the mass of the mobile species, as shown in Figure 10b. The activation energy (the ionic conductivity) decreases (increases) as the fractional volume (F) increases. It would be very interesting to see if this trend also holds for crystalline compounds. Recently, this descriptor has been used in a high-throughput calculation to find possible candidates of lithium-, sodium-, potassium-, silver and copper- ion conductors having potentially higher ionic conductivity.[177] This method has also been used to study crystalline lithium-ion conductors and electrodes, and by varying the threshold of the bond valence mismatch, researchers can get information not only about the diffusion pathways[178] but also the fraction of mobile lithium contributing to conduction as well as possible diffusion mechanisms that are dominant in

these materials.[179]

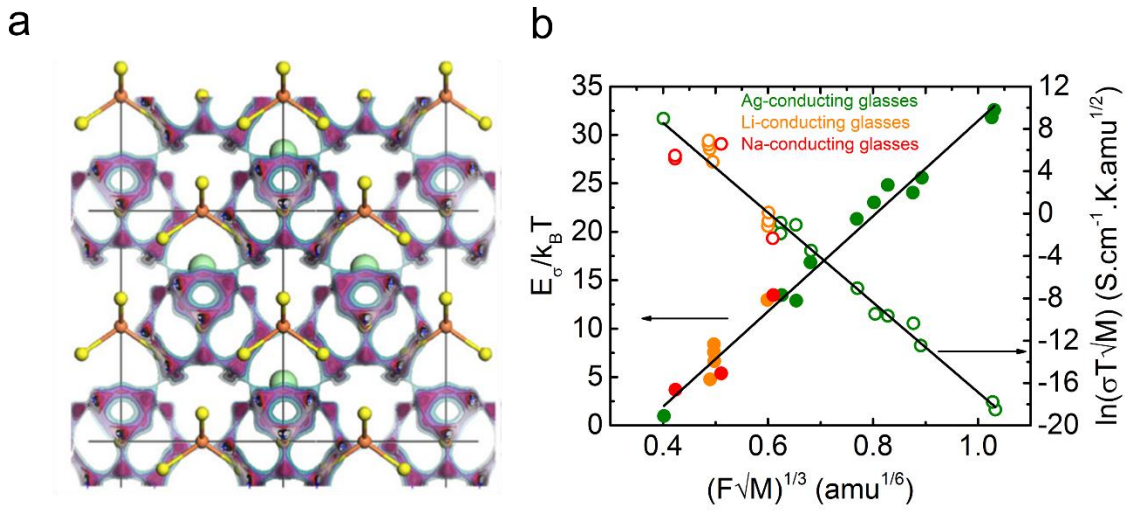

Figure 10. a) Lithium diffusion pathway in Li_6PS_5Cl. The yellow, orange, and cyan spheres represent sulfur, phosphorus, and chlorine atoms, respectively. Different colors of diffusion pathway correspond to different values of bond valence mismatch, from the highest in light blue to the lowest in red. Reprinted with permission from Rayavarapu et al. Copyright Springer 2012.[180] b). The correlation between the activation energy and ionic conductivity of Ag, Li, and Na-conducting glasses with the fractional volume of diffusion pathway F scaled by the square root of the mass of the mobile species M (e.g. M is the mass of Ag^+ in Ag-conducting glasses).[181]

The volume of the percolating diffusion pathway can also be determined by molecular dynamics simulations. Classical molecular dynamics was used to validate the threshold method reported in Figure 10, but the determination of the diffusion pathway volume by the more accurate ab-initio molecular dynamics is still lacking and would deserve future work. However, it is interesting to note that the shape of the percolating diffusion volume as estimated by the bond valence method is in close agreement with the lithium-ion distribution estimated by neutron diffraction data.[177]

4.2. Lattice Dynamics

When changing the ligand by moving down in the periodic table (i.e. chalcogens or halogens), the ionic conductivity of monovalent cations typically increases. As the electronegativity of the ligand decreases, we expect weaker attractive forces between the ligand and mobile cation. For example, changing the ligand from F^- to I^-, Ag^+ and Li^+ conductivity increases by many orders of magnitude in halides LiX (X = F, Cl, Br and I) and the olivine Li_2ZnM_4 (M = Cl, Br and I) as shown in Figure 11a. Interestingly, the increasing lithium-ion conductivity in halides from LiF to LiI can be correlated with increasing Li-X distance, halogen atom polarizability and reduced electronegativity of the halogen atom, as shown in Figure 11b. Notice that the ionic conductivity of the lithium argyrodites family seems to contradict this trend as the conductivity of Li_6PS_5I is the lowest in the series while according to this trend we expect it to be the highest (Figure 5). The reason for this apparent contradiction is the fact that in this family, in addition to halide anions, there are also sulfur anions that outnumber the halide anions by a ratio 5 to 1 per formula unit. Therefore, we expect the S^{2-} to have a more significant impact on ionic conductivity than halide anions. Indeed, the conductivity of Li_6PO_5Cl is several order of magnitudes lower than its sulfur-containing counterpart (see Figure 5).

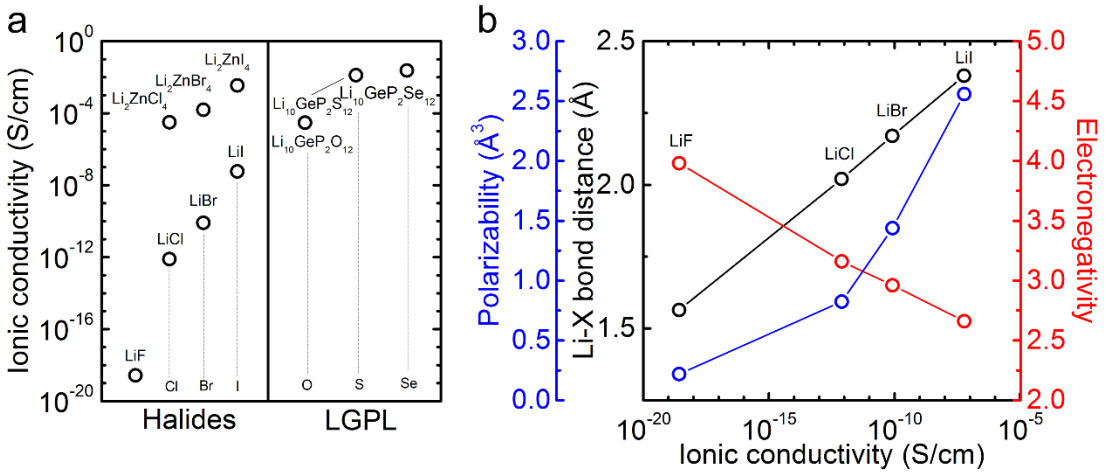

Figure 11. a) Ionic conductivity for structures with varying anions/ligands (crystalline lithium halides (T = 400 K),[182] olivine Li_2ZnM_4 (M = Cl,[183] Br[184] and I[185]) (T = 523 K) and lithium superionic conductors $Li_{10}GeP_2L_{12}$ (L = O, S and Se) at room temperature[115]). b) Halogen-atom polarizability (Å^3),[186] Li-halide bond distance (Å),[186] and halogen electronegativity (Pauling scale)[187] as a function of lithium-ion

conductivity at 400 K for lithium halides (F, Cl, Br and I).[182] Bond length and polarizability values were obtained from the National Institute of Standards and Technology (NIST).[186] Electronegativity values are presented in Pauling scale and were obtained from reference.[187]

The substitution of oxygen by sulfur in the γ-Li_3PO_4 type structure to form thio-LISICON leads to an increase of several orders of magnitude in the lithium-ion conductivity.[81] Several computational studies,[188,189] mostly using density functional theory (DFT), are in agreement with this experimental finding. These studies have also revealed that the enhancement of ionic conductivity upon substitution of O by S is a generic feature in phosphate compounds as it has been shown to be equally valid for the compounds $Li_7P_3O_{11}$ and $Li_7P_3S_{11}$ as well as $Li_4P_2O_7$ and $Li_4P_2S_7$.[190] Similar trends in enhanced lithium-ion mobility (reduced activation energy) have been found computationally for the $Li_{10}GeP_2X_{12}$ (X=O, S, or Se) family going from O to S or Se.[115] Again, this trend is in agreement with the concept shown in Figure 11b as S^{2-} and Se^{2-} are larger and have a higher polarizability than O^{2-}, confirming this approach as an effective strategy to increase ionic conductivity in solid-state lithium-ion conductors.

The existence of a correlation between the polarizability and the activation energy hints at other related correlations since the polarizability can be linked to other physical parameters. In particular, it can be related to high-frequency dielectric constant ε_∞ *via* the well-known Clausius-Mossotti relation (in the case of cubic binary compounds)[191]:

$$\frac{\varepsilon_\infty - 1}{\varepsilon_\infty + 2} = \frac{4\pi\alpha}{3V_a} \qquad (4)$$

Where α is the sum of the polarizability of the ions in the primitive cell and V_a is the volume of the primitive cell. Indeed, Wakamura found that there is nonlinear correlation between the activation energy and the high-frequency dielectric constant ε_∞ for Ag^+, F^-, Li^+ and a few Na^+, Cu^+ as well as Cl^- conductors shown in Figure 12a,[192] the activation energy being decreased with increasing ε_∞. Similarly, the correlation between activation energy and ε_∞ hints at the existence of other descriptors that are related to ε_∞. In

particular, the frequency of the transverse optical phonon ω_{TO} can be related to ε_∞ using the Lyddane-Sachs-Teller relation[191]:

$$\frac{\omega_{TO}^2}{\omega_{LO}^2} = \frac{\varepsilon_\infty}{\varepsilon_o} \qquad (5)$$

Where ω_{LO} is the frequency of the longitudinal optical mode and ε_o is the static dielectric constant. As expected, a correlation between the activation energy and ω_{TO} (equivalent to ω_{LEO}, frequency of the low-energy optical mode) has been found as shown in Figure 12b. The activation energy decreases with decreasing ω_{TO} in agreement with the idea that low phonon frequency is associated with large vibration amplitude, hence increasing the probability of the mobile species to hop to the neighboring lattice site.[193] It is interesting to note that similar correlation also exists between the enthalpy of migration and the frequency of longitudinal acoustic phonon at $2/3\,\langle 111\rangle$ in the Brillouin zone in body-centered cubic metals.[194]

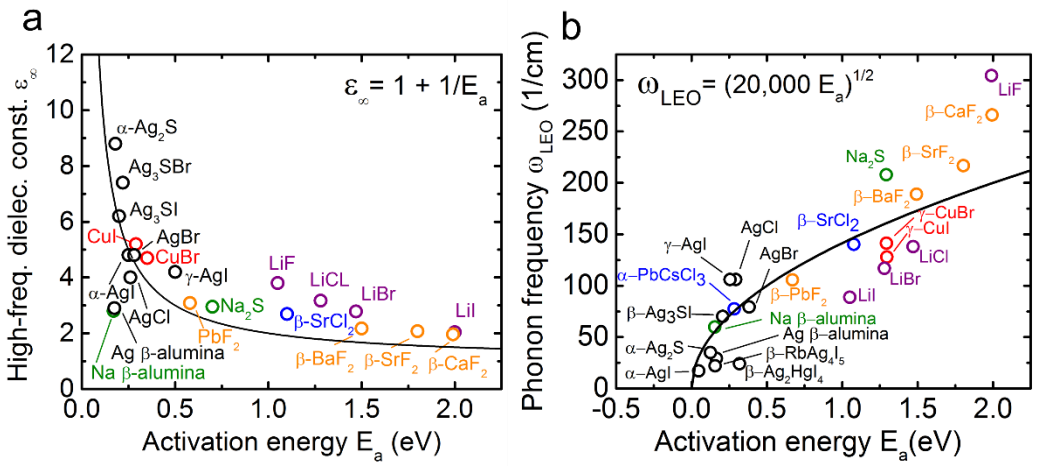

Figure 12. Correlation between activation energy and a) high-frequency dielectric constant ϵ_∞ [192]and b) frequency of low-energy optical phonon ω_{LEO}.[193] The activation energy increases with increasing ω_{LEO} and decreasing ϵ_∞. Lithium-halide activation energies are from [182], dielectric constants from [191], and phonon low-energy optical frequency from previous work.[195] The equations in each figure correspond to the solid lines which were fitted with the data in the figures and plotted as the guide to the eyes.

The above descriptors could be used to screen and design crystalline materials with increased bulk

ionic conductivity. However, the progresses in the experimental technique in terms of materials synthesis and nanostructure preparation open additional routes to design optimized lithium conductors by engineering the interfacial properties. The modification of the lattice volume by means of interfacial strain described in Section 3.6 is an example and other examples are described in the following section.

5. Size-Tailored Ionic Conductivities

The interfaces between materials (grain boundaries, separation between different phases, or surfaces) represent a structural discontinuity that is accompanied by changes in charge carrier concentration. Ionic conductivity can be influenced by the net electrostatic charge present at the interface.[196] At grain boundaries the resulting effect is often detrimental for the conductivity. On the interface between two different materials such unbalanced charge would generate space charge regions in proximity of the interface, with an accumulation of (interstitial) mobile species (for ex. lithium-ions in lithium conductors) on one side and a depletion of mobile species (or equivalently, an accumulation of vacancies) on the other side.[196-200] This charge accumulation/depletion is due to the difference in the electrochemical potential of the mobile species at the interface, causing a net migration of charge across the boundary, a phenomenon similar to the build up of p-n junction which is well-known in semiconductor physics.

The increase in the concentration of the mobile species at the interfaces enhances the ionic conductivity. This concept is supported by the ionic conductivities and activation energy of undoped epitaxial BaF_2/CaF_2 multilayers with different layer thicknesses, as shown in Figure 13a.[201] As the layers become thinner, the relative volume affected by the space charge layer becomes increasingly large, resulting in higher concentration of charge carriers and increased ionic conductivity[201]. However, in heavily doped ion conductors such as YSZ, the space charge layer is expected to be very thin and its effect on conductivity becomes negligible. For example, 8 mol% YSZ has the space charge thickness of the order of 2 - 3 nm at 500 °C.[202]

Recent advances on nanosized bulk ion conductors can potentially take advantage of ion conduction along interfaces.[197] In nano-sized systems, where the volume of the interfacial zones constitutes several tenths of the total volume, interfacial ion conductivity can dominate.[196,203] Examples can be found in the heterogeneous doping of halides (LiX) and Li_2ZnI_4 when nanoporous alumina is employed as second phase, where 3 or 4 orders of magnitudes of lithium-ion conductivity enhancement can be obtained, as shown in Figure 13b.[103,203,204]

A similar effect has been recently observed for nanoporous Li_3PS_4, which shows an ionic conductivity 1.6×10^{-4} S/cm at room temperature,[205] much higher than the reported ionic conductivity for this material in bulk form (Figure 5a). This drastic increase in ionic conductivity has been attributed partly to a preference for the more conductive β-Li_3PS_4 phase (intrinsic bulk ionic conductivity of 8.93×10^{-7} S/cm)[205], but especially to the surface conductivity. The surface conductivity, demonstrated by the correlation between the surface area and the ionic conductivity, is believed to be triggered by the space charge at the surface which promotes lithium vacancy diffusion.[205]

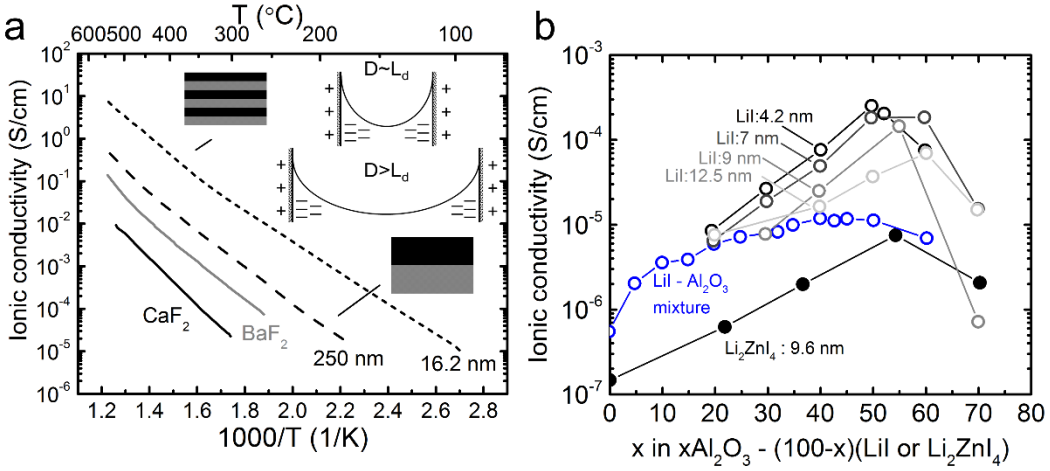

Figure 13. a) Conductivity as a function of temperature for CaF_2-BaF_2 superlattices (dotted lines) as well as bulk CaF_2 and BaF_2 (solid lines).[201] Inset) Space charge layers for distances (D) between interfaces on the order of the Debye length (L_d) and for distances much larger than the Debye length. b) Lithium

conductivity as a function of LiI[204] or Li_2ZnI_4[103] fraction in ordered mesoporous alumina (Al_2O_3) composite for different pore sizes. The conductivity of LiI-Al_2O_3 homogenous mixture is also shown for comparison.[206]

6. Conclusion and Future Perspectives

In this review, we highlight the interplay between ionic size and lattice volume that is shown to greatly influence ionic conductivity in a number of structural families. Diffusion coefficients of mobile monovalent ions can exhibit a volcano trend with the ionic radius within a given structure, where the maximum diffusion coefficients and lowest migration energies can be achieved with an optimum size. This observation can be rationalized by the arguments that the diffusion of ions that are too large can be limited by moving through structural bottlenecks and ions that are too small can become trapped in potential minima. This concept has been used extensively to enhance lithium-ion conductivity within the LISICON-like, NASICON-like and perovskite families, where increasing lattice volume by substitution can be correlated with larger bottleneck sizes, reduced activation energies and greater ionic conductivity by several orders of magnitude. In addition to controlling lattice volume by substitution, ionic conductivity can be enhanced by increasing lattice volume via mechanically imposed strains, which has been shown to enhance oxygen-ion conduction but not yet for lithium-ion conduction.

We discuss opportunities in establishing descriptors of ionic conductivities, which can universally correlate with ionic conductivity across different families of structures, which have the potential to greatly accelerate the discovery of new ion conductors with superionic conductivity. Electrolytes with body-centered cubic anion sub-lattices[207] and structures where the mobile species is not in its preferred coordination have been correlated with high ionic conductivity[208] and suggested to be a promising route for locating new superionic conductors. Increasing the volume of the ion diffusion pathway determined from the bond valence method of silver-, sodium- and lithium-ion-conducting glasses correlates with reduced activation energy and enhanced ionic conductivity.[181] In addition, increasing the high-frequency dielectric constant and lowering the frequency of the low-energy optical phonons is shown to enhance ionic

conductivities among different ionic conductors including silver-, sodium-, lithium- and fluorine-ion conduction.[192,193] Further experimental and computational work is needed to test these hypotheses.

While a number of solid-state electrolytes have ionic conductivities approaching that of liquid electrolytes, the reactivity between solid-state electrolytes and electrode materials[115,144,148] limits practical use of solid-state electrolytes in lithium-ion batteries, which is poorly understood. Future work is needed to understand the reaction mechanisms at the interface between fast lithium-ion conductors and conventional lithium-ion electrode materials, and between two different fast lithium-ion conductors, and develop solutions to stabilize these interfaces. Such understanding and control of interfacial reactivity is essential to realize the opportunities of exploiting space charge layers created in multi-component ion conductors to enhance ion conductivity by nanostructural designs,[196] and minimizing interface reactivity by protecting lithium-ion conductors with surface coatings.

Acknowledgements

J.C.B is supported in part from the National Science Foundation Graduate Research Fellowship (1122374) and H.-H. C is in part supported from the Ministry of Science and Technology of Taiwan (102-2917-I-564-006-A1). Research support at MIT from BMW and the Skoltech-MIT Center on Electrochemical Energy is acknowledged.

Supplementary Information Available: Details on types of defects, measurement techniques, and structural schematics are provided. Supplementary tables on the values used to extrapolate conductivities from high to low temperatures is given. Supplementary figure on the relation between the bottleneck size and lattice volume for NASICON-like conductors is shown.

Conflict of Interest Disclosure: The authors declare no competing financial interest.

Biographies

John Christopher Bachman holds B.S and M.S. degrees in Mechanical Engineering from University of California, Davis. He is currently a PhD. candidate in Mechanical Engineering at MIT working in the Electrochemical Energy Lab under Prof. Yang Shao-Horn, studying lithium solid-state electrolytes.

Sokseiha Muy received his B.S. and M.S. degrees in Material Sciences from École Polytechnique, France. He is currently a PhD. student in the Department of Materials Science and Engineering at MIT working in the Electrochemical Energy Lab under Prof. Yang Shao-Horn. His research interest includes the design principle of new solid-state electrolytes for Li-ion battery.

Alexis Grimaud is an associate researcher at Collège de France in Paris, France. He received his physical-chemistry engineering diploma from the Graduate School of Chemistry and Physics of Bordeaux in 2008 and his PhD from the University of Bordeaux in 2011. He then was postdoctoral associate at MIT from 2012 to 2014 working in the Electrochemical Energy Lab with Prof. Yang Shao-Horn. In 2014, he joined Prof. Jean-Marie Tarascon's research group at Collège de France, Paris, France as an associate researcher. His research interests are in the understanding of anionic redox and the design of new materials for water splitting, metal-air and Li-ion batteries.

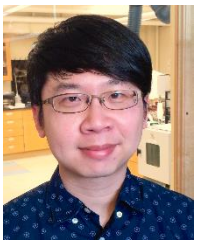

Hao-Hsun Chang received his B.S., M.S., and PhD. degrees in chemical engineering from National Taiwan University. He is now a postdoctoral fellow/associate in Prof. Yang Shao-Horn's group at MIT.

Prior to joining the Electrochemical Energy Lab, he was a senior engineer at China Petrochemical Development Corporation from 2010 to 2012 and a principal engineer at Taiwan Semiconductor Manufacturing Company in 2013. His current researches center on synthesis and characterizations of solid-state electrolytes for lithium-ion and metal-air batteries.

Nir Pour is currently a postdoctoral associate at MIT in the Electrochemical Energy Lab. His research centers on vanadium redox flow batteries. He hold a BSc degree in Biophysics and an MSc and PhD. in chemistry researching magnesium batteries under the supervision of Prof. Doron Aurbach, from Bar-Ilan University in Israel.

Peter Lamp received his MSc in physics from the Technical University of Munich in 1989. In 1993, he obtained his PhD in general physics. His PhD thesis "Investigation of photoelectric injection of electrons in liquid argon" was prepared at the Max Planck Institute for Physics, Munich. Between 1994 and 2000 he was group leader at the Department of Energy Conversion and Storage of the Bayerischen Zentrum für angewandte Energieforschung (ZAE) in Garching. After a short period as project leader for fuel cell systems at Webasto Thermo Systems International GmbH, he joined BMW AG in 2001 as a development engineer for fuel cell systems.
Since 2004 he has been leader of the "Technology and Concepts Electric Energy Storage" group and, since 2012, of the "Battery Technology" department at BMW.

Odysseas Paschos has studied Physics at the Aristotle University of Thessaloniki in Greece. In 2008 he obtained his PhD on Materials Science from College of Nanoscale Science and Engineering at SUNY Albany and moved to Munich, Germany where he worked at the Technische Universität München (TUM) as a Post-Doctoral Associate in the Physics Department. During this period, he worked on several aspects of electrical conversion of storage including synthesis and electrochemical characterization of materials related to fuel cells and batteries. Since 2012 he is working at BMW in the group Research Battery Technology lead by Dr. Peter Lamp and is in charge of the Material projects investigating potential candidates and technologies for future automotive cells.

Saskia Lupart received her MSc. degree in Chemistry from the Ludwig-Maximilians-Universität München (LMU), Germany. In 2012 she completed her PhD studies in solid-state chemistry at the LMU. Since 2012 she is working at BMW AG at the group of Dr. Peter Lamp in the "Research Battery Technology" section where she is in charge of solid-state electrolytes for lithium batteries.

Simon Lux obtained a MSc. degree in Technical Chemistry from the Technical University of Graz, Austria and completed his PhD studies in Physical Chemistry at the University of Muenster, Germany. After two years at the Lawrence Berkeley National Laboratory, Simon joined BMW of North America as Advanced Battery Engineer. In his current role, he is responsible for the coordination and management of the lithium-ion battery technology projects from the material to the cell level in the NAFTA region and engages in technology scouting in the USA.

Filippo Maglia was an assistant professor at the Chemistry Department of the University of Pavia, Italy between 2005 and 2012. He received his PhD in chemistry from the University of Pavia in 1998. Dr. Maglia has spent several periods as visiting scientist between 1998 and 2005 at the department of chemical engineering and materials science of the University of California Davis. In 2009 he was DAAD fellow at the Technische Universität München, Germany. In 2013 he joined BMW AG at the group of Dr. Peter Lamp in the "Research Battery Technology" department and is working on topics related to lifetime aspects of battery materials.

Livia Giordano has been an assistant professor at the Material Science Department of University of Milano-Bicocca in Italy since 2007, and since September 2013 is also visiting professor at MIT. She obtained her PhD in Material Science from the University of Milano-Bicocca in 2002 and she was a visiting scientist at the CNRS of Marseille and the University College of London. After starting as an experimental scientist, her research has then focused on first-principles calculations of surface reactivity of oxides, and interfacial phenomena at metal-oxide and oxide-liquid interfaces.

Yang Shao-Horn is W.M. Keck Professor of Energy, Professor of Mechanical Engineering and Professor of Materials Science and Engineering at MIT. Her interests include surface science, catalysis/electrocatalysis, and design of electron and phonon structures of materials for electrochemical energy storage, solid state ionics, photoelectrochemical conversion and clean environmental applications. Professor Shao-Horn has published around 200 research articles and mentored/trained over 50 M.S. and Ph.D. graduate students and postdoctoral associates at MIT.

References

(1) Minh, N. Q. Ceramic Fuel Cells. *J. Am. Ceram. Soc.* **1993**, *76*, 563-588.

(2) Jensen, J.; Krebs, F. C. From the Bottom Up - Flexible Solid State Electrochromic Devices. *Adv. Mater.* **2014**, *26*, 7231-7234.

(3) Traversa, E. Ceramic Sensors For Humidity Detection - The State-Of-The-Art And Future-Developments. *Sens. Actuator B-Chem.* **1995**, *23*, 135-156.

(4) Yamazoe, N.; Miura, N. Environmental Gas-Sensing. *Sens. Actuator B-Chem.* **1994**, *20*, 95-102.

(5) Strukov, D. B.; Snider, G. S.; Stewart, D. R.; Williams, R. S. The Missing Memristor Found. *Nature* **2008**, *453*, 80-83.

(6) Ferrari, S.; Loveridge, M.; Beattie, S. D.; Jahn, M.; Dashwood, R. J.; Bhagat, R. Latest Advances In The Manufacturing Of 3D Rechargeable Lithium Microbatteries. *J. Power Sources* **2015**, *286*, 25-46.

(7) Tarascon, J. M.; Armand, M. Issues and Challenges Facing Rechargeable Lithium Batteries. *Nature* **2001**, *414*, 359-367.

(8) Tubandt, C. Über Elektrizitätsleitung in Festen Kristallisierten Verbindungen. Zweite Mitteilung. Überführung und Wanderung der Ionen in Einheitlichen Festen Elektrolyten. *Z. Anorg. Allg. Chem.* **1921**, *115*, 105-126.

(9) Bradley, J. N.; Greene, P. D. Solids with High Ionic Conductivity in Group 1 Halide Systems. *Trans. of Far. Soc.* **1967**, *63*, 424-430.

(10) Goodenough, J. B.; Hong, H. Y. P.; Kafalas, J. A. Fast Na^+-Ion Transport in Skeleton Structures. *Mater. Res. Bull.* **1976**, *11*, 203-220.

(11) Briant, J. L.; Farrington, G. C. Ionic Conductivity in Na^+, K^+, and Ag^+ β″-Alumina. *J. Solid State Chem.* **1980**, *33*, 385-390.

(12) Adachi, G.-y.; Imanaka, N.; Tamura, S. Ionic Conducting Lanthanide Oxides. *Chem. Rev.* **2002**, *102*, 2405-2430.

(13) Rodger, A. R.; Kuwano, J.; West, A. R. Li^+ ion conducting γ solid solutions in the systems Li_4XO_4-Li_3YO_4: X=Si, Ge, Ti; Y=P, As, V; Li_4XO_4-$LiZO_2$: Z=Al, Ga, Cr and Li_4GeO_4-Li_2CaGeO_4. *Solid State Ionics* **1985**, *15*, 185-198.

(14) Deiseroth, H.-J.; Kong, S.-T.; Eckert, H.; Vannahme, J.; Reiner, C.; Zaiß, T.; Schlosser, M. Li_6PS_5X: A Class of Crystalline Li-Rich Solids With an Unusually High Li^+ Mobility. *Angew. Chem. Int. Ed.* **2008**, *47*, 755-758.

(15) Thangadurai, V.; Narayanan, S.; Pinzaru, D. Garnet-Type Solid-State Fast Li Ion Conductors for Li Batteries: Critical Review. *Chem. Soc. Rev.* **2014**, *43*, 4714-4727.

(16) Martínez-Juárez, A.; Pecharromán, C.; Iglesias, J. E.; Rojo, J. M. Relationship between Activation Energy and Bottleneck Size for Li^+ Ion Conduction in NASICON Materials of Composition $LiMM'(PO_4)_3$; M, M' = Ge, Ti, Sn, Hf. *J. Phys. Chem. B* **1998**, *102*, 372-375.

(17) Yamane, H.; Kikkawa, S.; Koizumi, M. Preparation Of Lithium Silicon Nitrides And Their Lithium Ion Conductivity. *Solid State Ionics* **1987**, *25*, 183-191.

(18) Schnick, W.; Luecke, J. Lithium Ion Conductivity of $LiPN_2$ and Li_7PN_4. *Solid State Ionics* **1990**, *38*, 271-273.

(19) Matsuo, M.; Oguchi, H.; Maekawa, H.; Takamura, H.; Orimo, S. Complex Hydrides: A New Category of Solid-State Lithium Fast-Ion Conductors. *Material Matters* **2010**, *5*.

(20) Bohnke, O.; Bohnke, C.; Fourquet, J. L. Mechanism Of Ionic Conduction And Electrochemical Intercalation Of Lithium Into The Perovskite Lanthanum Lithium Titanate. *Solid State Ionics* **1996**, *91*, 21-31.

(21) Stramare, S.; Thangadurai, V.; Weppner, W. Lithium Lanthanum Titanates: A Review. *Chem. Mater.* **2003**, *15*, 3974-3990.

(22) Lutz, H. D.; Kuske, P.; Wussow, K. Ionic Motion Of Tetrahedrally And Octahedrally Coordinated Lithium Ions In Ternary And Quaternary Halides. *Solid State Ionics* **1988**, *28–30, Part 2*, 1282-1286.

(23) Kanno, R.; Hata, T.; Kawamoto, Y.; Irie, M. Synthesis of a New Lithium Ionic conductor, Thio-LISICON–Lithium Germanium Sulfide System. *Solid State Ionics* **2000**, *130*, 97-104.

(24) Kamaya, N.; Homma, K.; Yamakawa, Y.; Hirayama, M.; Kanno, R.; Yonemura, M.; Kamiyama, T.; Kato, Y.; Hama, S.; Kawamoto, K.et al. A Lithium Superionic Conductor. *Nat Mater* **2011**, *10*, 682-686.

(25) Bron, P.; Johansson, S.; Zick, K.; Schmedt auf der Günne, J.; Dehnen, S.; Roling, B. $Li_{10}SnP_2S_{12}$: An Affordable Lithium Superionic Conductor. *J. Am. Chem. Soc.* **2013**, *135*, 15694-15697.

(26) Whiteley, J. M.; Woo, J. H.; Hu, E.; Nam, K.-W.; Lee, S.-H. Empowering the Lithium Metal Battery through a Silicon-Based Superionic Conductor. *J. Electrochem. Soc.* **2014**, *161*, A1812-A1817.

(27) Nazri, G. A.; Pistoia, G. *Lithium Batteries: Science and Technology*; Springer: New York, 2009, p 523.

(28) Armand, M.; Tarascon, J. M. Building Better Batteries. *Nature* **2008**, *451*, 652-657.

(29) Abraham, K. M. Directions in Secondary Lithium Battery Research-and-Development. *Electrochim. Acta* **1993**, *38*, 1233-1248.

(30) Wakihara, M. Recent Developments in Lithium Ion Batteries. *Mater. Sci. Eng. R-Rep.* **2001**, *33*, 109-134.

(31) Xu, K. Nonaqueous Liquid Electrolytes for Lithium-Based Rechargeable Batteries. *Chem. Rev.* **2004**, *104*, 4303-4418.

(32) Zugmann, S.; Fleischmann, M.; Amereller, M.; Gschwind, R. M.; Wiemhöfer, H. D.; Gores, H. J. Measurement of Transference Numbers for Lithium Ion Electrolytes Via Four Different Methods, A Comparative Study. *Electrochim. Acta* **2011**, *56*, 3926-3933.

(33) Weppner, W. In *Encyclopedia of Electrochemical Power Sources*; Garche, J., Ed.; Elsevier: Amsterdam, 2009; p 162-168.

(34) Takada, K. In *Encyclopedia of Electrochemical Power Sources*; Garche, J., Ed.; Elsevier: Amsterdam, 2009; p 328-336.

(35) Patil, A.; Patil, V.; Shin, D. W.; Choi, J. W.; Paik, D. S.; Yoon, S. J. Issue and Challenges Facing Rechargeable Thin Film Lithium Batteries. *Mater. Res. Bull.* **2008**, *43*, 1913-1942.

(36) Park, M.; Zhang, X. C.; Chung, M. D.; Less, G. B.; Sastry, A. M. A Review of Conduction Phenomena in Li-Ion Batteries. *J. Power Sources* **2010**, *195*, 7904-7929.

(37) Jung, Y.-C.; Kim, S.-K.; Kim, M.-S.; Lee, J.-H.; Han, M.-S.; Kim, D.-H.; Shin, W.-C.; Ue, M.; Kim, D.-W. Ceramic separators based on Li^+-conducting inorganic electrolyte for high-performance lithium-ion batteries with enhanced safety. *J. Power Sources* **2015**, *293*, 675-683.

(38) Goodenough, J. B.; Kim, Y. Challenges for Rechargeable Li Batteries. *Chem. Mater.* **2009**, *22*, 587-603.

(39) Kurzweil, P.; Brandt, K. In *Encyclopedia of Electrochemical Power Sources*; Garche, J., Ed.; Elsevier: Amsterdam, 2009; p 1-26.

(40) Hassoun, J.; Verrelli, R.; Reale, P.; Panero, S.; Mariotto, G.; Greenbaum, S.; Scrosati, B. A Structural, Spectroscopic and Electrochemical Study of a Lithium Ion Conducting $Li_{10}GeP_2S_{12}$ Solid Electrolyte. *J. Power Sources* **2013**, *229*, 117-122.

(41) Tobishima, S. In *Encyclopedia of Electrochemical Power Sources*; Garche, J., Ed.; Elsevier: Amsterdam, 2009; p 409-417.

(42) Roth P., O. C. How Electrolytes Influence Battery Safety. *Electrochem. Soc. Interface* **Summer 2012**.

(43) Feng, J. K.; Lu, L.; Lai, M. O. Lithium Storage Capability of Lithium Ion Conductor $Li_{1.5}Al_{0.5}Ge_{1.5}(PO_4)_3$. *J. Alloys Compd.* **2010**, *501*, 255-258.

(44) Sandhya, C. P.; John, B.; Gouri, C. Lithium Titanate as Anode Material for Lithium-Ion Cells: A Review. *Ionics* **2014**, *20*, 601-620.

(45) Knauth, P. Inorganic Solid Li Ion Conductors: An Overview. *Solid State Ionics* **2009**, *180*, 911-916.

(46) Saruwatari, H.; Kuboki, T.; Kishi, T.; Mikoshiba, S.; Takami, N. Imidazolium Ionic Liquids Containing LiBOB Electrolyte for Lithium Battery. *J. Power Sources* **2010**, *195*, 1495-1499.

(47) Croce, F.; Appetecchi, G. B.; Persi, L.; Scrosati, B. Nanocomposite Polymer Electrolytes for Lithium Batteries. *Nature* **1998**, *394*, 456-458.

(48) Yu, X.; Bates, J. B.; Jellison, G. E.; Hart, F. X. A Stable Thin-Film Lithium Electrolyte: Lithium Phosphorus Oxynitride. *J. Electrochem. Soc.* **1997**, *144*, 524-532.

(49) Inaguma, Y.; Liquan, C.; Itoh, M.; Nakamura, T.; Uchida, T.; Ikuta, H.; Wakihara, M. High Ionic Conductivity in Lithium Lanthanum Titanate. *Solid State Commun.* **1993**, *86*, 689-693.

(50) Bernuy-Lopez, C.; Manalastas, W.; Lopez del Amo, J. M.; Aguadero, A.; Aguesse, F.; Kilner, J. A. Atmosphere Controlled Processing of Ga-Substituted Garnets for High Li-Ion Conductivity Ceramics. *Chem. Mater.* **2014**, *26*, 3610-3617.

(51) Yung-Fang Yu, Y.; Kummer, J. T. Ion Exchange Properties of and Rates of Ionic Diffusion in Beta-Alumina. *J. Inorg. Nucl. Chem.* **1967**, *29*, 2453-2475.

(52) Levi, E.; Gofer, Y.; Aurbach, D. On the Way to Rechargeable Mg Batteries: The Challenge of New Cathode Materials. *Chem. Mater.* **2009**, *22*, 860-868.

(53) Higashi, S.; Miwa, K.; Aoki, M.; Takechi, K. A Novel Inorganic Solid State Ion Conductor for Rechargeable Mg Batteries. *Chem. Commun.* **2014**, *50*, 1320-1322.

(54) Bonne, R. W.; Schoonman, J. The Ionic Conductivity of Beta Lead Fluoride. *J. Electrochem. Soc.* **1977**, *124*, 28-35.

(55) Schoonman, J.; Oversluizen, G.; Wapenaar, K. E. D. Solid Electrolyte Properties of LaF_3. *Solid State Ionics* **1980**, *1*, 211-221.

(56) Hu, Z.; Xie, K.; Wei, D.; Ullah, N. Influence of Sputtering Pressure on the Structure and Ionic Conductivity of Thin Film Amorphous Electrolyte. *J Mater Sci* **2011**, *46*, 7588-7593.

(57) Souquet, J. L. Ionic Transport in Amorphous Solid Electrolytes. *Annu. Rev. Mater. Sci.* **1981**, *11*, 211-231.

(58) Tärneberg, R.; Lundn, A. Ion Diffusion in the High-Temperature Phases Li_2SO_4, $LiNaSO_4$, $LiAgSO_4$ and $Li_4Zn(SO_4)_3$. *Solid State Ionics* **1996**, *90*, 209-220.

(59) Lide, D. R.; Frederikse, H. P. R. *CRC Handbook of Chemistry and Physics*; CRC Press, 1994, Ch 5 p 93.

(60) Bockris, J. O. M.; Reddy, A. K. N.; Gamboa-Aldeco, M. *Modern Electrochemistry 1: Ionics*; Springer, Ch 4, 1998.

(61) Kummer, J. T. β-Alumina Electrolytes. *Prog. Solid State Chem.* **1972**, *7*, 141-175.

(62) Buck, R. P. Transfort Properties of Ionic Conductors. *Sensors Actuators* **1981**, *1*, 137-196.

(63) Goodenough, J. B. Oxide-Ion Electrolytes. *Ann. Rev. Mat.. Res.* **2003**, *33*, 91-128.

(64) Hull, S. Superionics: Crystal Structures and Conduction Processes. *Rep. Prog. Phys.* **2004**, *67*, 1233.

(65) McWhan, D. B.; Allen, S. J.; Remeika, J. P.; Dernier, P. D. Ion-Ion Correlations and Diffusion in β-Alumina. *Phys. Rev. Lett.* **1975**, *35*, 953-956.

(66) Kawai, H.; Kuwano, J. Lithium Ion Conductivity of A-Site Deficient Perovskite Solid Solution $La_{0.67-x}Li_{3x}TiO_3$. *J. Electrochem. Soc.* **1994**, *141*, L78-L79.

(67) Shannon, R. D. Revised Effective Ionic Radii and Systematic Studies of Interatomic Distances in Halides and Chalcogenides. *Acta Crystallogr A* **1976**, *32*, 751-767.

(68) Aono, H.; Sugimoto, E.; Sadaoka, Y.; Imanaka, N.; Adachi, G. y. Ionic Conductivity of Solid Electrolytes Based on Lithium Titanium Phosphate. *J. Electrochem. Soc.* **1990**, *137*, 1023-1027.

(69) Strickler, D. W.; Carlson, W. G. Ionic Conductivity of Cubic Solid Solutions in the System $CaO—Y_2O_3—ZrO_2$. *J. Am. Ceram. Soc.* **1964**, *47*, 122-127.

(70) Bauerle, J. E. Study of Solid Electrolyte Polarization by a Complex Admittance Method. *J. Phys. Chem. Solids* **1969**, *30*, 2657-2670.

(71) van Dijk, T.; Burggraaf, A. J. Grain Boundary Effects on Ionic Conductivity in Ceramic $Gd_xZr_{1-x}O2_{-(x/2)}$ Solid Solutions. *Phys. Status Solidi A* **1981**, *63*, 229-240.

(72) Bruce, P. G.; West, A. R. The AC Conductivity of Polycrystalline LISICON, $Li_{2+2x}Zn_{1-x}GeO_4$, and a Model for Intergranular Constriction Resistances. *J. Electrochem. Soc.* **1983**, *130*, 662-669.

(73) Fleig, J.; Maier, J. A Finite Element Study on the Grain Boundary Impedance of Different Microstructures. *J. Electrochem. Soc.* **1998**, *145*, 2081-2089.

(74) Fleig, J.; Maier, J. Finite-Element Calculations on the Impedance of Electroceramics with Highly Resistive Grain Boundaries: I, Laterally Inhomogeneous Grain Boundaries. *J. Am. Ceram. Soc.* **1999**, *82*, 3485-3493.

(75) Guo, X.; Maier, J. Grain Boundary Blocking Effect in Zirconia: A Schottky Barrier Analysis. *J. Electrochem. Soc.* **2001**, *148*, E121-E126.

(76) Moriwake, H.; Gao, X.; Kuwabara, A.; Fisher, C. A. J.; Kimura, T.; Ikuhara, Y. H.; Kohama, K.; Tojigamori, T.; Ikuhara, Y. Domain boundaries and their influence on Li migration in solid-state electrolyte $(La,Li)TiO_3$. *J. Power Sources* **2015**, *276*, 203-207.

(77) Chung, H.; Kang, B. Increase in grain boundary ionic conductivity of $Li_{1.5}Al_{0.5}Ge_{1.5}(PO_4)_3$ by adding excess lithium. *Solid State Ionics* **2014**, *263*, 125-130.

(78) Yubuchi, S.; Teragawa, S.; Aso, K.; Tadanaga, K.; Hayashi, A.; Tatsumisago, M. Preparation of high lithium-ion conducting Li_6PS_5Cl solid electrolyte from ethanol solution for all-solid-state lithium batteries. *J. Power Sources* **2015**, *293*, 941-945.

(79) Kanno, R.; Murayama , M. Lithium Ionic Conductor Thio-LISICON: The Li_2S GeS_2 P_2S_5 System. *J. Electrochem. Soc.* **2001**, *148*, A742-A746.

(80) Rao, R. P.; Adams, S. Studies of Lithium Argyrodite Solid Electrolytes for All-Solid-State Batteries. *Phys. Status Solidi A* **2011**, *208*, 1804-1807.

(81) Tachez, M.; Malugani, J.-P.; Mercier, R.; Robert, G. Ionic Conductivity of and Phase Transition in Lithium Thiophosphate Li_3PS_4. *Solid State Ionics* **1984**, *14*, 181-185.

(82) Murayama, M.; Kanno, R.; Irie, M.; Ito, S.; Hata, T.; Sonoyama, N.; Kawamoto, Y. Synthesis of New Lithium Ionic Conductor Thio-LISICON—Lithium Silicon Sulfides System. *J. Solid State Chem.* **2002**, *168*, 140-148.

(83) Deng, Y.; Eames, C.; Chotard, J.-N.; Lalère, F.; Seznec, V.; Emge, S.; Pecher, O.; Grey, C. P.; Masquelier, C.; Islam, M. S. Structural and Mechanistic Insights into Fast Lithium-Ion Conduction in Li_4SiO_4–Li_3PO_4 Solid Electrolytes. *J. Am. Chem. Soc.* **2015**, *137*, 9136-9145.

(84) Boulineau, S.; Courty, M.; Tarascon, J.-M.; Viallet, V. Mechanochemical Synthesis of Li-Argyrodite Li_6PS_5X (X=Cl, Br, I) as Sulfur-Based Solid Electrolytes for All Solid State Batteries Application. *Solid State Ionics* **2012**, *221*, 1-5.

(85) Pecher, O.; Kong, S.-T.; Goebel, T.; Nickel, V.; Weichert, K.; Reiner, C.; Deiseroth, H.-J.; Maier, J.; Haarmann, F.; Zahn, D. Atomistic Characterisation of Li^+ Mobility and Conductivity in $Li_{7-x}PS_{6-x}I_x$ Argyrodites from Molecular Dynamics Simulations, Solid-State NMR, and Impedance Spectroscopy. *Chem. Eur. J.* **2010**, *16*, 8347-8354.

(86) Deiseroth, H.-J.; Maier, J.; Weichert, K.; Nickel, V.; Kong, S.-T.; Reiner, C. Li_7PS_6 and Li_6PS_5X (X: Cl, Br, I): Possible Three-dimensional Diffusion Pathways for Lithium Ions and Temperature Dependence of the Ionic Conductivity by Impedance Measurements. *Z. Anorg. Allg. Chem.* **2011**, *637*, 1287-1294.

(87) Kong, S.-T.; Deiseroth, H.-J.; Maier, J.; Nickel, V.; Weichert, K.; Reiner, C. Li_6PO_5Br and Li_6PO_5Cl: The First Lithium-Oxide-Argyrodites *Z. Anorg. Allg. Chem.* **2010**, *636*, 1920-1924.

(88) Buschmann, H.; Dolle, J.; Berendts, S.; Kuhn, A.; Bottke, P.; Wilkening, M.; Heitjans, P.; Senyshyn, A.; Ehrenberg, H.; Lotnyk, A.et al. Structure and Dynamics of the Fast Lithium Ion Conductor "$Li_7La_3Zr_2O_{12}$". *PCCP* **2011**, *13*, 19378-19392.

(89) Thangadurai, V.; Weppner, W. $Li_6ALa_2Ta_2O_{12}$ (A = Sr, Ba): Novel Garnet-Like Oxides for Fast Lithium Ion Conduction. *Adv. Funct. Mater.* **2005**, *15*, 107-112.

(90) Peng, H.; Wu, Q.; Xiao, L. Low Temperature Synthesis of $Li_5La_3Nb_2O_{12}$ with Cubic Garnet-Type Structure by Sol–Gel Process. *J. Sol-Gel Sci. Technol.* **2013**, *66*, 175-179.

(91) Gao, Y. X.; Wang, X. P.; Wang, W. G.; Fang, Q. F. Sol–Gel Synthesis and Electrical Properties of $Li_5La_3Ta_2O_{12}$ Lithium Ionic Conductors. *Solid State Ionics* **2010**, *181*, 33-36.

(92) Aono, H.; Sugimoto, E.; Sadaoka, Y.; Imanaka, N.; Adachi, G. y. The Electrical Properties of Ceramic Electrolytes for $LiM_xTi_{2-x}(PO_4)_3 + yLi_2O$, M = Ge, Sn, Hf, and Zr Systems. *J. Electrochem. Soc.* **1993**, *140*, 1827-1833.

(93) Boukamp, B. A.; Huggins, R. A. Fast Ionic Conductivity in Lithium Nitride. *Mater. Res. Bull.* **1978**, *13*, 23-32.

(94) Matsuo, M.; Nakamori, Y.; Orimo, S.-i.; Maekawa, H.; Takamura, H. Lithium Superionic Conduction in Lithium Borohydride Accompanied by Structural Transition. *Appl. Phys. Lett.* **2007**, *91*, 224103.

(95) Boukamp, B. A.; Huggins, R. A. Ionic Conductivity in Lithium Imide. *Phys. Lett. A* **1979**, *72*, 464-466.

(96) Oguchi, H.; Matsuo, M.; Sato, T.; Takamura, H.; Maekawa, H.; Kuwano, H.; Orimo, S. Lithium-Ion Conduction in Complex Hydrides $LiAlH_4$ and Li_3AlH_6. *J. Appl. Phys.* **2010**, *107*, 096104.

(97) Matsuo, M.; Sato, T.; Miura, Y.; Oguchi, H.; Zhou, Y.; Maekawa, H.; Takamura, H.; Orimo, S.-i. Synthesis and Lithium Fast-Ion Conductivity of a New Complex Hydride $Li_3(NH_2)_2I$ with Double-Layered Structure. *Chem. Mater.* **2010**, *22*, 2702-2704.

(98) Morata-Orrantia, A.; García-Martín, S.; Morán, E.; Alario-Franco, M. Á. A New $La_{2/3}Li_xTi_{1-x}Al_xO_3$ Solid Solution: Structure, Microstructure, and Li^+ Conductivity. *Chem. Mater.* **2002**, *14*, 2871-2875.

(99) Thangadurai, V.; Shukla, A. K.; Gopalakrishnan, J. $LiSr_{1.65} \cdot {}_{0.35}B_{1.3}B'_{1.7}O_9$ (B = Ti, Zr; B' = Nb, Ta): New Lithium Ion Conductors Based on the Perovskite Structure. *Chem. Mater.* **1999**, *11*, 835-839.

(100) Itoh, M.; Inaguma, Y.; Jung, W.-H.; Chen, L.; Nakamura, T. High Lithium Ion Conductivity in the Perovskite-Type Compounds $Ln_{12}Li_{12}TiO_3$ (Ln=La,Pr,Nd,Sm). *Solid State Ionics* **1994**, *70–71, Part 1*, 203-207.

(101) Lutz, H. D.; Schmidt, W.; Haeuseler, H. Chloride Spinels: A New Group of Solid Lithium Electrolytes. *J. Phys. Chem. Solids* **1981**, *42*, 287-289.

(102) Lutz, H. D.; Zhang, Z.; Pfitzner, A. Fast Ionic Conductivity of Ternary Iodides in the Systems LiI-$M^{II}I_2$ (M^{II}=Mn, Cd, Pb). *Solid State Ionics* **1993**, *62*, 1-3.

(103) Maekawa, H.; Iwatani, T.; Shen, H.; Yamamura, T.; Kawamura, J. Enhanced Lithium Ion Conduction and the Size Effect on Interfacial Phase in Li_2ZnI_4–Mesoporous Alumina Composite Electrolyte. *Solid State Ionics* **2008**, *178*, 1637-1641.

(104) Hahn, T. *International Tables for Crystallography, Space-Group Symmetry*; Wiley, Dordrecht, 2005.

(105) West A, R. Crystal Chemistry of Some Tetrahedral Oxides. *Z. Kristallogr.* **1975**, *141*, 422.

(106) Du, Y. A.; Holzwarth, N. A. W. Mechanisms of Li^+ Diffusion in Crystalline γ- and β-Li_3PO_4 Electrolytes from First Principles. *Phys. Rev. B* **2007**, *76*, 174302.

(107) Shannon, R. D.; Taylor, B. E.; English, A. D.; Berzins, T. New Li Solid Electrolytes. *Electrochim. Acta* **1977**, *22*, 783-796.

(108) Hu, Y. W.; Raistrick, I. D.; Huggins, R. A. Ionic Conductivity of Lithium Orthosilicate—Lithium Phosphate Solid Solutions. *J. Electrochem. Soc.* **1977**, *124*, 1240-1242.

(109) Hong, H. Y. P. Crystal structure and ionic conductivity of Li14Zn(GeO4)4 and other new Li+ superionic conductors. *Mater. Res. Bull.* **1978**, *13*, 117-124.

(110) Kuhn, A.; Gerbig, O.; Zhu, C.; Falkenberg, F.; Maier, J.; Lotsch, B. V. A New Ultrafast Superionic Li-Conductor: Ion Dynamics in $Li_{11}Si_2PS_{12}$ and Comparison with Other Tetragonal LGPS-Type Electrolytes. *PCCP* **2014**, *16*, 14669-14674.

(111) Kuhn, A.; Kohler, J.; Lotsch, B. V. Single-crystal X-ray structure analysis of the superionic conductor Li10GeP2S12. *PCCP* **2013**, *15*, 11620-11622.

(112) Hu, C. H.; Wang, Z. Q.; Sun, Z. Y.; Ouyang, C. Y. Insights Into Structural Stability and Li Superionic Conductivity of $Li_{10}GeP_2S_{12}$ from First-Principles Calculations. *Chem. Phys. Lett.* **2014**, *591*, 16-20.

(113) Mo, Y.; Ong, S. P.; Ceder, G. First Principles Study of the $Li_{10}GeP_2S_{12}$ Lithium Super Ionic Conductor Material. *Chem. Mater.* **2011**, *24*, 15-17.

(114) Kato, Y.; Saito, R.; Sakano, M.; Mitsui, A.; Hirayama, M.; Kanno, R. Synthesis, Structure and Lithium Ionic Conductivity of Solid Solutions of $Li_{10}(Ge_{1-x}M_x)P_2S_{12}$ (M = Si, Sn). *J. Power Sources* **2014**, *271*, 60-64.

(115) Ong, S. P.; Mo, Y.; Richards, W. D.; Miara, L.; Lee, H. S.; Ceder, G. Phase Stability, Electrochemical Stability and Ionic Conductivity of the $Li_{10+/-1}MP_2X_{12}$ (M = Ge, Si, Sn, Al or P, and X = O, S or Se) Family of Superionic Conductors. *Energy Environ. Sci.* **2013**, *6*, 148-156.

(116) Du, F.; Ren, X.; Yang, J.; Liu, J.; Zhang, W. Structures, Thermodynamics, and Li^+ Mobility of $Li_{10}GeP_2S_{12}$: A First-Principles Analysis. *J. Phys. Chem. C* **2014**, *118*, 10590-10595.

(117) Epp, V.; Gün, Ö.; Deiseroth, H.-J.; Wilkening, M. Highly Mobile Ions: Low-Temperature NMR Directly Probes Extremely Fast Li^+ Hopping in Argyrodite-Type Li_6PS_5Br. *J. Phys. Chem. Lett.* **2013**, *4*, 2118-2123.

(118) Chen, M.; Rao, R. P.; Adams, S. High Capacity All-Solid-State Cu–Li_2S/Li_6PS_5Br/In Batteries. *Solid State Ionics* **2014**, *262*, 183-187.

(119) Rao, R. P.; Sharma, N.; Peterson, V. K.; Adams, S. Formation and Conductivity Studies of Lithium Argyrodite Solid Electrolytes Using In-Situ Neutron Diffraction. *Solid State Ionics* **2013**, *230*, 72-76.

(120) Ortiz, G. F.; López, M. C.; Lavela, P.; Vidal-Abarca, C.; Tirado, J. L. Improved Lithium-Ion Transport in NASICON-Type Lithium Titanium Phosphate by Calcium and Iron Doping. *Solid State Ionics* **2014**, *262*, 573-577.

(121) Subramanian, M. A.; Subramanian, R.; Clearfield, A. Lithium Ion Conductors in the System $AB(IV)_2(PO_4)_3$ (B = Ti, Zr and Hf). *Solid State Ionics* **1986**, *18–19, Part 1*, 562-569.

(122) Kubanska, A.; Castro, L.; Tortet, L.; Schäf, O.; Dollé, M.; Bouchet, R. Elaboration of Controlled Size $Li_{1.5}Al_{0.5}Ge_{1.5}(PO_4)_3$ Crystallites from Glass-Ceramics. *Solid State Ionics* **2014**, *266*, 44-50.

(123) Thangadurai, V.; K. Shukla, A.; Gopalakrishnan, J. New Lithium-Ion Conductors Based on the NASICON Structure. *J. Mater. Chem.* **1999**, *9*, 739-741.

(124) Norhaniza, R.; Subban, R. H. Y.; Mohamed, N. S. Cr and V Substituted $LiSn_2P_3O_{12}$ Solid Electrolyte Materials. *J. Power Sources* **2013**, *244*, 300-305.

(125) Arbi, K.; Hoelzel, M.; Kuhn, A.; García-Alvarado, F.; Sanz, J. Structural Factors That Enhance Lithium Mobility in Fast-Ion $Li_{1+x}Ti_{2-x}Al_x(PO_4)_3$ ($0 \leq x \leq 0.4$) Conductors Investigated by Neutron Diffraction in the Temperature Range 100–500 K. *Inorg. Chem.* **2013**, *52*, 9290-9296.

(126) Arbi, K.; Tabellout, M.; Lazarraga, M. G.; Rojo, J. M.; Sanz, J. Non-Arrhenius Conductivity in the Fast Lithium Conductor. *Phys. Rev. B* **2005**, *72*, 094302.

(127) Cretin, M.; Fabry, P. Comparative Study of Lithium Ion Conductors in the System $Li_{1+x}Al_xA_{2-x}^{IV}(PO_4)_3$ with A^{IV}=Ti or Ge and $0 \leq x \leq 0{\cdot}7$ for use as Li^+ sensitive membranes. *J. Eur. Ceram. Soc.* **1999**, *19*, 2931-2940.

(128) Cao, C.; Li, Z.; Wang, X.-L.; Zhao, X.; Han, W.-Q. Recent advances in inorganic solid electrolytes for lithium batteries. *Frontiers in Energy Research* **2014**, *2*.

(129) Hartmann, P.; Leichtweiss, T.; Busche, M. R.; Schneider, M.; Reich, M.; Sann, J.; Adelhelm, P.; Janek, J. Degradation of NASICON-Type Materials in Contact with Lithium Metal:

Formation of Mixed Conducting Interphases (MCI) on Solid Electrolytes. *J. Phys. Chem. C* **2013**, *117*, 21064-21074.

(130) O'Callaghan, M. P.; Lynham, D. R.; Cussen, E. J.; Chen, G. Z. Structure and Ionic-Transport Properties of Lithium-Containing Garnets $Li_3Ln_3Te_2O_{12}$ (Ln = Y, Pr, Nd, Sm−Lu). *Chem. Mater.* **2006**, *18*, 4681-4689.

(131) Cussen, E. J.; Yip, T. W. S.; O'Neill, G.; O'Callaghan, M. P. A Comparison of the Transport Properties of Lithium-Stuffed Garnets and the Conventional Phases $Li_3Ln_3Te_2O_{12}$. *J. Solid State Chem.* **2011**, *184*, 470-475.

(132) Ramzy, A.; Thangadurai, V. Tailor-Made Development of Fast Li Ion Conducting Garnet-Like Solid Electrolytes. *ACS Appl. Mater. Interfaces* **2010**, *2*, 385-390.

(133) Thangadurai, V.; Kaack, H.; Weppner, W. J. F. Novel Fast Lithium Ion Conduction in Garnet-Type $Li_5La_3M_2O_{12}$ (M = Nb, Ta). *J. Am. Ceram. Soc.* **2003**, *86*, 437-440.

(134) Thangadurai, V.; Weppner, W. $Li_6ALa_2Nb_2O_{12}$ (A=Ca, Sr, Ba): A New Class of Fast Lithium Ion Conductors with Garnet-Like Structure. *J. Am. Ceram. Soc.* **2005**, *88*, 411-418.

(135) Cussen, E. J. The Structure of Lithium Garnets: Cation Disorder and Clustering in a New Family of Fast Li^+ Conductors. *Chem. Commun.* **2006**, 412-413.

(136) Cussen, E. J. Structure and Ionic Conductivity in Lithium Garnets. *J. Mater. Chem.* **2010**, *20*, 5167-5173.

(137) Ramakumar, S.; Satyanarayana, L.; Manorama, S. V.; Murugan, R. Structure and Li^+ Dynamics of Sb-doped $Li_7La_3Zr_2O_{12}$ Fast Lithium Ion Conductors. *PCCP* **2013**, *15*, 11327-11338.

(138) Miara, L. J.; Ong, S. P.; Mo, Y.; Richards, W. D.; Park, Y.; Lee, J.-M.; Lee, H. S.; Ceder, G. Effect of Rb and Ta Doping on the Ionic Conductivity and Stability of the Garnet $Li_{7+2x-y}(La_{3-x}Rb_x)(Zr_{2-y}Ta_y)O_{12}$ ($0 \leq x \leq 0.375$, $0 \leq y \leq 1$) Superionic Conductor: A First Principles Investigation. *Chem. Mater.* **2013**, *25*, 3048-3055.

(139) Awaka, J.; Kijima, N.; Hayakawa, H.; Akimoto, J. Synthesis and Structure Analysis of Tetragonal $Li_7La_3Zr_2O_{12}$ with the Garnet-Related Type Structure. *J. Solid State Chem.* **2009**, *182*, 2046-2052.

(140) Wolfenstine, J.; Rangasamy, E.; Allen, J. L.; Sakamoto, J. High Conductivity of Dense Tetragonal $Li_7La_3Zr_2O_{12}$. *J. Power Sources* **2012**, *208*, 193-196.

(141) Kumazaki, S.; Iriyama, Y.; Kim, K.-H.; Murugan, R.; Tanabe, K.; Yamamoto, K.; Hirayama, T.; Ogumi, Z. High Lithium Ion Conductive $Li_7La_3Zr_2O_{12}$ by Inclusion of Both Al and Si. *Electrochem. Commun.* **2011**, *13*, 509-512.

(142) El Shinawi, H.; Janek, J. Stabilization of Cubic Lithium-Stuffed Garnets of the Type "$Li_7La_3Zr_2O_{12}$" by Addition of Gallium. *J. Power Sources* **2013**, *225*, 13-19.

(143) Murugan, R.; Thangadurai, V.; Weppner, W. Fast Lithium Ion Conduction in Garnet-Type $Li_7La_3Zr_2O_{12}$. *Angew. Chem. Int. Ed.* **2007**, *46*, 7778-7781.

(144) Kim, K. H.; Iriyama, Y.; Yamamoto, K.; Kumazaki, S.; Asaka, T.; Tanabe, K.; Fisher, C. A. J.; Hirayama, T.; Murugan, R.; Ogumi, Z. Characterization of the interface between LiCoO2 and Li7La3Zr2O12 in an all-solid-state rechargeable lithium battery. *J. Power Sources* **2011**, *196*, 764-767.

(145) Harada, Y.; Ishigaki, T.; Kawai, H.; Kuwano, J. Lithium Ion Conductivity of Polycrystalline Perovskite $La_{0.67-x}Li_{3x}TiO_3$ with Ordered and Disordered Arrangements of the A-Site Ions. *Solid State Ionics* **1998**, *108*, 407-413.

(146) Jay, E. E.; Rushton, M. J. D.; Chroneos, A.; Grimes, R. W.; Kilner, J. A. Genetics of Superionic Conductivity in Lithium Lanthanum Titanates. *PCCP* **2015**, *17*, 178-183.

(147) Thangadurai, V.; Weppner, W. Effect of B-site Substitution of $(Li,La)TiO_3$ Perovskites by Di-, Tri-, Tetra- and Hexavalent Metal Ions on the Lithium Ion Conductivity. *Ionics* **2000**, *6*, 70-77.

(148) Wenzel, S.; Leichtweiss, T.; Krüger, D.; Sann, J.; Janek, J. Interphase formation on lithium solid electrolytes—An in situ approach to study interfacial reactions by photoelectron spectroscopy. *Solid State Ionics* **2015**, *278*, 98-105.

(149) Khorassani, A.; West, A. R. New Li^+ Ion Conductors in the System Li_4SiO_4−Li_3AsO_4. *Solid State Ionics* **1982**, *7*, 1-8.

(150) Khorassani, A.; West, A. R. Li^+ Ion Conductivity in the System Li_4SiO_4-Li_3VO_4. *J. Solid State Chem.* **1984**, *53*, 369-375.

(151) Arbi, K.; Rojo, J. M.; Sanz, J. Lithium Mobility in Titanium Based Nasicon $Li_{1+x}Ti_{2-x}Al_x(PO_4)_3$ and $LiTi_{2-x}Zr_x(PO_4)_3$ Materials Followed by NMR and Impedance Spectroscopy. *J. Eur. Ceram. Soc.* **2007**, *27*, 4215-4218.

(152) Guo, X.; Maier, J. Ionically Conducting Two-Dimensional Heterostructures. *Adv. Mater.* **2009**, *21*, 2619-2631.

(153) Fabbri, E.; Pergolesi, D.; Traversa, E. Ionic Conductivity in Oxide Heterostructures: The Role of Interfaces. *Science and Technology of Advanced Materials* **2010**, *11*, 054503.

(154) Leon, C.; Santamaria, J.; Boukamp, B. A. Oxide Interfaces with Enhanced Ion Conductivity. *MRS Bull.* **2013**, *38*, 1056-1063.

(155) Yildiz, B. "Stretching" the energy landscape of oxides—Effects on electrocatalysis and diffusion. *MRS Bull.* **2014**, *39*, 147-156.

(156) Kim, D. H.; Imashuku, S.; Wang, L.; Shao-Horn, Y.; Ross, C. A. Li Loss During the Growth of (Li,La)TiO_3 Thin Films by Pulsed Laser Deposition. *J. Cryst. Growth* **2013**, *372*, 9-14.

(157) Aguesse, F.; Roddatis, V.; Roqueta, J.; García, P.; Pergolesi, D.; Santiso, J.; Kilner, J. A. Microstructure and Ionic Conductivity of LLTO Thin Films: Influence of Different Substrates and Excess Lithium in the Target. *Solid State Ionics* **2015**, *272*, 1-8.

(158) Ohnishi, T.; Takada, K. Synthesis and Orientation Control of Li-Ion Conducting Epitaxial $Li_{0.33}La_{0.56}TiO_3$ Solid Electrolyte Thin Films by Pulsed Laser Deposition. *Solid State Ionics* **2012**, *228*, 80-82.

(159) Kim, S.; Hirayama, M.; Cho, W.; Kim, K.; Kobayashi, T.; Kaneko, R.; Suzuki, K.; Kanno, R. Low Temperature Synthesis and Ionic Conductivity of the Epitaxial $Li_{0.17}La_{0.61}TiO_3$ Film Electrolyte. *Cryst. Eng. Comm.* **2014**, *16*, 1044-1049.

(160) Kim, S.; Hirayama, M.; Suzuki, K.; Kanno, R. Hetero-Epitaxial Growth of $Li_{0.17}La_{0.61}TiO_3$ Solid Electrolyte on $LiMn_2O_4$ Electrode for All Solid-State Batteries. *Solid State Ionics* **2014**, *262*, 578-581.

(161) Wei, J.; Ogawa, D.; Fukumura, T.; Hirose, Y.; Hasegawa, T. Epitaxial Strain-Controlled Ionic Conductivity in Li-Ion Solid Electrolyte $Li_{0.33}La_{0.56}TiO_3$ Thin Films. *Cryst. Growth Des.* **2015**, *15*, 2187-2191.

(162) Schichtel, N.; Korte, C.; Hesse, D.; Janek, J. Elastic Strain at Interfaces and its Influence on Ionic Conductivity in Nanoscaled Solid Electrolyte Thin Films-Theoretical Considerations and Experimental Studies. *PCCP* **2009**, *11*, 3043-3048.

(163) Korte, C.; Peters, A.; Janek, J.; Hesse, D.; Zakharov, N. Ionic Conductivity and Activation Energy for Oxygen Ion Transport in Superlattices-The Semicoherent Multilayer System YSZ (ZrO_2 + 9.5 mol% Y_2O_3)/Y_2O_3. *PCCP* **2008**, *10*, 4623-4635.

(164) Li, F.; Lu, R.; Wu, H.; Kan, E.; Xiao, C.; Deng, K.; Ellis, D. E. The Strain Effect on Colossal Oxygen Ionic Conductivity in Nanoscale Zirconia Electrolytes: A First-Principles-Based Study. *PCCP* **2013**, *15*, 2692-2697.

(165) Schichtel, N.; Korte, C.; Hesse, D.; Zakharov, N.; Butz, B.; Gerthsen, D.; Janek, J. On the Influence of Strain on Ion Transport: Microstructure and Ionic Conductivity of Nanoscale YSZ|Sc_2O_3 Multilayers. *PCCP* **2010**, *12*, 14596-14608.

(166) Jiang, J.; Hu, X.; Shen, W.; Ni, C.; Hertz, J. L. Improved Ionic Conductivity in Strained Yttria-Stabilized Zirconia Thin Films. *Appl. Phys. Lett.* **2013**, *102*, -.

(167) Aydin, H.; Korte, C.; Rohnke, M.; Janek, J. Oxygen Tracer Diffusion Along Interfaces of Strained Y_2O_3/YSZ Multilayers. *PCCP* **2013**, *15*, 1944-1955.

(168) Gerstl, M.; Friedbacher, G.; Kubel, F.; Hutter, H.; Fleig, J. The Relevance of Interfaces for Oxide Ion Transport in Yttria Stabilized Zirconia (YSZ) Thin Films. *PCCP* **2013**, *15*, 1097-1107.

(169) Pergolesi, D.; Fabbri, E.; Cook, S. N.; Roddatis, V.; Traversa, E.; Kilner, J. A. Tensile Lattice Distortion Does Not Affect Oxygen Transport in Yttria-Stabilized Zirconia–CeO_2 Heterointerfaces. *ACS Nano* **2012**, *6*, 10524-10534.

(170) Pennycook, T. J.; Beck, M. J.; Varga, K.; Varela, M.; Pennycook, S. J.; Pantelides, S. T. Origin of Colossal Ionic Conductivity in Oxide Multilayers: Interface Induced Sublattice Disorder. *Phys. Rev. Lett.* **2010**, *104*, 115901.

(171) Fronzi, M.; Cereda, S.; Tateyama, Y.; De Vita, A.; Traversa, E. Ab Initio Investigation of Defect Formation at ZrO_2-CeO_2 Interfaces. *Phys. Rev. B* **2012**, *86*, 085407.

(172) Inaguma, Y.; Chen, L.; Itoh, M.; Nakamura, T. Candidate Compounds with Perovskite Structure for High Lithium Ionic Conductivity. *Solid State Ionics* **1994**, *70–71, Part 1*, 196-202.

(173) Rettenwander, D.; Geiger, C. A.; Tribus, M.; Tropper, P.; Amthauer, G. A Synthesis and Crystal Chemical Study of the Fast Ion Conductor $Li_{7-3x}Ga_xLa_3Zr_2O_{12}$ with x = 0.08 to 0.84. *Inorg. Chem.* **2014**, *53*, 6264-6269.

(174) Xu, B.; Duan, H.; Xia, W.; Guo, Y.; Kang, H.; Li, H.; Liu, H. Multistep sintering to synthesize fast lithium garnets. *J. Power Sources* **2016**, *302*, 291-297.

(175) Adams, S.; Swenson, J. Determining Ionic Conductivity from Structural Models of Fast Ionic Conductors. *Phys. Rev. Lett.* **2000**, *84*, 4144-4147.

(176) Brown, I. D. Recent Developments in the Methods and Applications of the Bond Valence Model. *Chem. Rev.* **2009**, *109*, 6858-6919.

(177) Avdeev, M.; Sale, M.; Adams, S.; Rao, R. P. Screening of the Alkali-Metal Ion Containing Materials from the Inorganic Crystal Structure Database (ICSD) for High Ionic Conductivity Pathways Using the Bond Valence Method. *Solid State Ionics* **2012**, *225*, 43-46.

(178) Filsø, M. Ø.; Turner, M. J.; Gibbs, G. V.; Adams, S.; Spackman, M. A.; Iversen, B. B. Visualizing Lithium-Ion Migration Pathways in Battery Materials. *Chem. Eur. J.* **2013**, *19*, 15535-15544.

(179) Adams, S. Bond Valence Analysis of Structure–Property Relationships in Solid Electrolytes. *J. Power Sources* **2006**, *159*, 200-204.

(180) Rayavarapu, P.; Sharma, N.; Peterson, V.; Adams, S. Variation in Structure and Li^+-Ion Migration in Argyrodite-Type Li_6PS_5X (X = Cl, Br, I) Solid Electrolytes. *J. Solid State Electrochem.* **2012**, *16*, 1807-1813.

(181) Adams, S.; Swenson, J. Bond Valence Analysis of Transport Pathways in RMC Models of Fast Ion Conducting Glasses. *PCCP* **2002**, *4*, 3179-3184.

(182) Haven, Y. The Ionic Conductivity of Li-Halide Crystals. *Recl. Trav. Chim. Pays-Bas* **1950**, *69*, 1471-1489.

(183) Lutz Heinz, D.; Wussow, K.; Kuske, P. In *Z. Naturforsch. B* 1987; Vol. 42, p 1379.

(184) Pfitzner, A.; Crockcroft, J. K.; Solinas, I.; Lutz, H. D. Neue Halogenozinkate(II) $M^{I2}ZnX_4$ (M^I = Li, Na; X = Cl, Br) mit Olivinstruktur. *Z. Anorg. Allg. Chem.* **1993**, *619*, 993-998.

(185) Lutz Heinz, D.; Pfitzner, A. In *Z. Naturforsch. B* 1989; Vol. 44, p 1047.

(186) Johnson III, R. D. NIST Computational Chemistry Comparison and Benchmark Database. NIST Standard Reference Database Number 101. Published Online: Release 16a, August 2013. http://cccbdb.nist.gov.

(187) Atkins, P.; de Paula, J. *Physical Chemistry*; W. H. Freeman: New York, 2006.

(188) Du, Y. A.; Holzwarth, N. A. W. Li Ion Diffusion Mechanisms in the Crystalline Electrolyte γ-Li_3PO_4. *J. Electrochem. Soc.* **2007**, *154*, A999-A1004.

(189) Lepley, N. D.; Holzwarth, N. A. W.; Du, Y. J. A. Structures, Li^+ Mobilities, and Interfacial Properties of Solid Electrolytes Li_3PS_4 and Li_3PO_4 from First Principles. *Phys. Rev. B* **2013**, *88*.

(190) Lepley, N.; Holzwarth, N. Computer Modeling of Crystalline Electrolytes - Lithium Thiophosphates and Phosphates. *ECS Trans.* **2011**, *35*, 39-51.

(191) Ashcroft, N. W.; Mermin, N. D. *Solid State Physics*; Holt, Rinehart and Winston, 1976.

(192) Wakamura, K. Effects of Electronic Band on Activation Energy and of Effective Charge on Lattice Distortion in Superionic Conductors. *J. Phys. Chem. Solids* **1998**, *59*, 591-598.

(193) Wakamura, K. Roles of Phonon Amplitude and Low-Energy Optical Phonons on Superionic Conduction. *Phys. Rev. B* **1997**, *56*, 11593-11599.

(194) Köhler, U.; Herzig, C. On the Correlation Between Self-Diffusion and the Low-Frequency LA ⅔<111> Phonon Mode in b.c.c. Metals. *Philos. Mag. A* **1988**, *58*, 769-786.

(195) Bilz, H.; Kress, W. *Phonon Dispersion Relations in Insulators*; Springer-Verlag, 1979.

(196) Maier, J. Ionic Conduction in Space Charge Regions. *Prog. Solid State Chem.* **1995**, *23*, 171-263.

(197) Tuller, H. L. Ionic Conduction in Nanocrystalline Materials. *Solid State Ionics* **2000**, *131*, 143-157.

(198) Kim, S.; Maier, J. On the Conductivity Mechanism of Nanocrystalline Ceria. *J. Electrochem. Soc.* **2002**, *149*, J73-J83.

(199) Maier, J. Defect Chemistry and Ionic Conductivity in Thin Films. *Solid State Ionics* **1987**, *23*, 59-67.

(200) Lupetin, P.; Gregori, G.; Maier, J. Mesoscopic Charge Carriers Chemistry in Nanocrystalline $SrTiO_3$. *Angew. Chem. Int. Ed.* **2010**, *49*, 10123-10126.

(201) Sata, N.; Eberman, K.; Eberl, K.; Maier, J. Mesoscopic Fast Ion Conduction in Nanometre-Scale Planar Heterostructures. *Nature* **2000**, *408*, 946-949.

(202) Guo, X. Can We Achieve Significantly Higher Ionic Conductivity in Nanostructured Zirconia? *Scripta Mater.* **2011**, *65*, 96-101.

(203) Maier, J. Size Effects on Mass Transport and Storage in Lithium Batteries. *J. Power Sources* **2007**, *174*, 569-574.

(204) Maekawa, H.; Tanaka, R.; Sato, T.; Fujimaki, Y.; Yamamura, T. Size-Dependent Ionic Conductivity Observed for Ordered Mesoporous Alumina-LiI Composite. *Solid State Ionics* **2004**, *175*, 281-285.

(205) Liu, Z.; Fu, W.; Payzant, E. A.; Yu, X.; Wu, Z.; Dudney, N. J.; Kiggans, J.; Hong, K.; Rondinone, A. J.; Liang, C. Anomalous High Ionic Conductivity of Nanoporous β-Li_3PS_4. *J. Am. Chem. Soc.* **2013**, *135*, 975-978.

(206) Liang, C. C. Conduction Characteristics of the Lithium Iodide-Aluminum Oxide Solid Electrolytes. *J. Electrochem. Soc.* **1973**, *120*, 1289-1292.

(207) Wang, Y.; Richards, W. D.; Ong, S. P.; Miara, L. J.; Kim, J. C.; Mo, Y.; Ceder, G. Design principles for solid-state lithium superionic conductors. *Nat. Mater.* **2015**, *advance online publication*.

(208) Rong, Z.; Malik, R.; Canepa, P.; Sai Gautam, G.; Liu, M.; Jain, A.; Persson, K.; Ceder, G. Materials Design Rules for Multivalent Ion Mobility in Intercalation Structures. *Chem. Mater.* **2015**, *27*, 6016-6021.

TOC

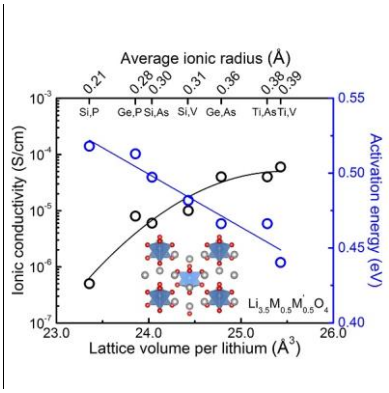

Inorganic Solid-State Electrolytes for Lithium Batteries: Mechanisms and Properties Governing Ion Conduction

John Christopher Bachman[1,2,‡], *Sokseiha Muy*[1,3,‡], *Alexis Grimaud*[1,4,‡], *Hao-Hsun Chang*[1,4], *Nir Pour*[1,4], *Simon F. Lux*[5], *Odysseas Paschos*[6], *Filippo Maglia*[6], *Saskia Lupart*[6], *Peter Lamp*[6], *Livia Giordano*[1,4,7] *and Yang Shao-Horn*[1,2,3,4] *

[1]Electrochemical Energy Laboratory, [2]Department of Mechanical Engineering, [3]Department of Materials Science and Engineering, [4]Research Laboratory of Electronics, Massachusetts Institute of Technology, Cambridge, Massachusetts 02139, United States

[5]BMW Group Technology Office USA, Mountain View, California 94043, United States

[6]BMW Group, Research Battery Technology, Munich, 80788, Germany

[7]Dipartimento di Scienza dei Materiali, Università di Milano-Bicocca, Milano, Italy

‡ These authors contributed equally

*email: shaohorn@mit.edu

A.G. current address: Chimie du Solide et Energie, FRE 3677, Collège de France, 75231 Paris Cedex 05, France or Réseau sur le Stockage Electrochimique de l'Energie (RS2E), FR CNRS 3459, 80039 Amiens Cedex, France

1. Types of Defects

2. Measurement Techniques

3. Structural Schematics

4. Supplementary Tables

5. Supplementary Figures

1. Types of Defects

In most of solids, the diffusion requires the presence of structural defects, like missing ions (vacancies) or ions located in interstitial positions. In pure solids, Schottky and Frenkel defects are generally those with the lowest energy of formation. When Schottky defects predominate, like in NaCl, diffusion occurs via random jumps between vacancy sites; in the case of Frenkel defects, direct interstitial jumps and interstitialcy migration (where the interstitial exchanges with the lattice ion) are possible, and the mechanism with lower activation energy dominates. The activation energy for diffusion in pure solids (E_A) depends on two contributions: the energy required to form the defect, E_f, and the energy required for the defect migration, E_m. E_m depends on the resistance offered by the host structure to the ion displacement from its initial to its final position, as illustrated in Figure S1. In particular E_m will reflect the energy required to overcome the saddle point position within the structure with the larger steric impediment (bottleneck). In the case of NaCl, as an example, the activation energy for Na^+ diffusion is determined by the energy required to cross the walls of octahedral anions. Since interstitial defects are most frequently observed in materials where one of the ions (the mobile species) is considerably smaller than the others, the corresponding activation energies are generally lower than those for vacancy diffusion.

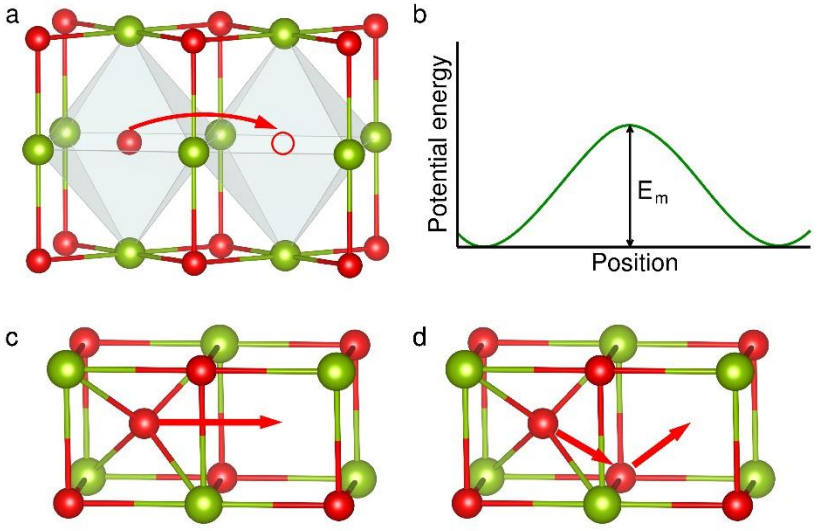

Figure S1. *Ion migration within a crystalline solid via a) vacancy, c) interstitial and d) interstitialcy mechanism. b) Potential energy profile for ion diffusion between two equivalent lattice sites.*

2. Measurement Techniques

The ionic conductivity in solid electrolytes is usually measured by impedance spectroscopy (AC technique), which applies a sinusoidal potential at various frequencies to an electrochemical cell with blocking electrodes and records its response. The complex impedance results can usually be analyzed using a combination of resistors, capacitors, Warburg, and constant-phase elements. A typical equivalent circuit for solid-state electrolytes can be composed of three RC-circuits, representing the bulk (or volume) conduction, grain boundary-conduction, and diffusion due to concentration gradient in the electrode, respectively from high to low frequencies.[3] Resistance from each portion can thus be extracted and the resulting ionic conductivity can be determined with a known thickness and area of the sample. This technique gives access to a microscopic diffusion value when the concentration of charge carriers is known.[1] Additionally, while measuring a sintered material, the measured conductivity or diffusion coefficient not only reflects the intrinsic properties of the material, but that of the grain boundaries. Indeed, the conductivity of grain boundaries can greatly differ from the bulk conductivity and the electrolyte resistance is in most cases the sum of bulk and grain boundary resistances, as evidenced for many polycrystalline electrolytes.

Other methods such as NMR spectroscopy (field-gradient NMR for direct diffusion for example) which allows collecting information from selective cations or anions,[2] quasielastic neutron scattering, or Mossbauer spectroscopy can also be employed to get access to microscopic information. Techniques such as DC conductivity, tracer diffusion, or relaxation techniques are sensitive to long-range diffusion and allow the measurement of a macroscopic diffusion coefficient. When the ionic conductor is subject to an external field or a gradient which can be chemical, electrical, or magnetic, the diffusion coefficient

measured is the chemical coefficient D_{Chem}. This coefficient differs from the self-diffusion coefficient or tracer diffusion coefficient D^* by a thermodynamic factor γ:[3]

$$D_{Chem} = \gamma D^* \qquad \text{(S1)}$$

γ being a measure of the deviation of the chemical activity from the ideal solution.

The transference number of the electrolyte—the ratio of the current carried by lithium ions to the sum of the current by all ions—is also an important parameter when assessing solid-state electrolytes. The transference number should be as high as possible to facilitate the transportation of lithium ions between electrodes. Fritz and Kuhn[4] have evaluated four different methods for measuring transference number of solid lithium electrolytes. They are known as AC complex impedance spectroscopy, steady-state current, isothermal transient ionic current, and Tubandt method, where each method has its own strengths and weaknesses, as described in their paper. In practice, the obvious difference of the electrochemical cells for these tests is the electrodes they use. When performing the measurement, non-blocking lithium electrodes are used in the former two techniques, so that cations in the solid electrolytes can continuously diffuse or migrate when a potential is applied. For the latter two techniques, they both use blocking electrodes, Pt for example, to let anions and cations be accumulated on the opposite sides of electrolyte when a potential is applied. The steady-state current method, developed by P. Bruce et al.,[5-7] has been extensively exploited. For the real measurement, a constant potential (ΔV) will be applied to a Li/Electrolyte/Li cell. The initial current (*Ii*) will slowly decrease to a steady-state current (*Iss*) and one can simply measure the resistance at initial (*Ri*) and steady state (*Rss*) by impedance spectroscopy. The transference number can be determined by:

$$t_+ = \frac{I_{SS}(\Delta V - I_i R_i)}{I_i(\Delta V - I_{ss} R_{SS})} \qquad \text{(S2)}$$

This technique is applicable not only for solid polymer[7] but also for organic electrolytes.[8]

Another important feature of a solid-state electrolyte is the ratio of the electrical conductivity to the lithium-ion conductivity. This value should be as close to zero as possible to stop leakage current between the two electrodes. To measure the electrical conductivity, one generally employs one blocking and one non-blocking electrode and measures the current at steady-state as a function of applied potential. As one electrode is blocking there is a buildup or depletion of mobile ions at the blocking electrode that offsets the applied electric potential. As a result, the current measured is purely electrical. This method is often referred to as the Hebb-Wagner method.[9-11]

3. Structural Schematics

Details of the structures described in section 3 of the main text are provided to help readers understand the details of each material.

a) LISICON-like (γ-Li_3PO_4)

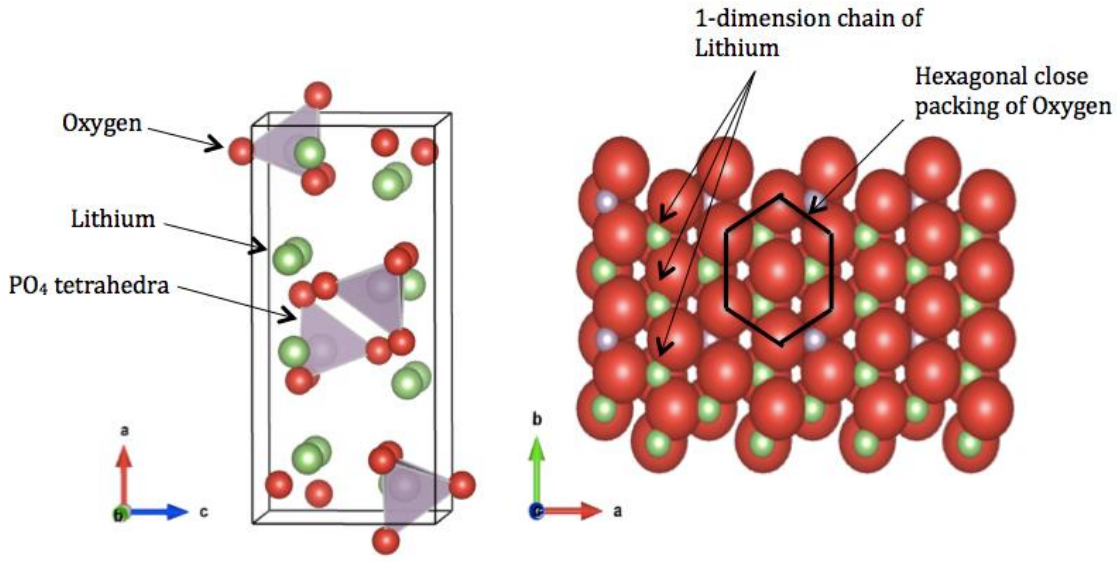

b) $Li_{10}GeP_2S_{12}$

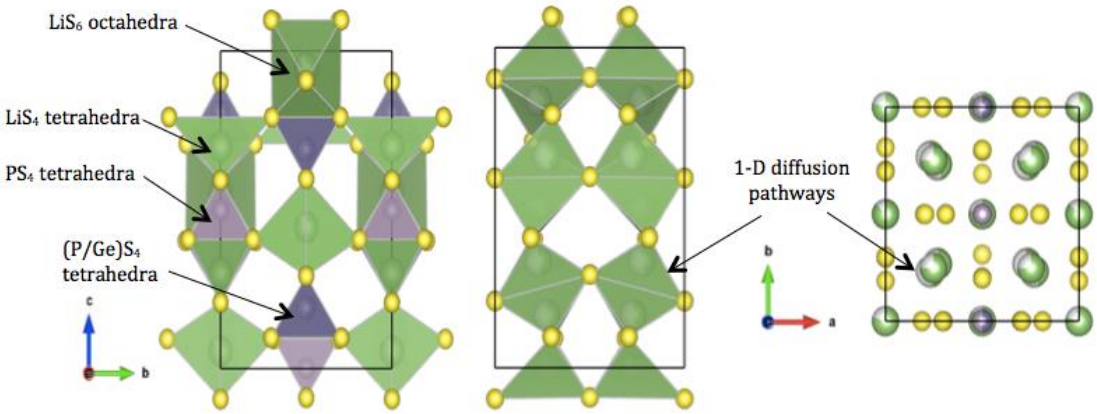

c) Argyrodite

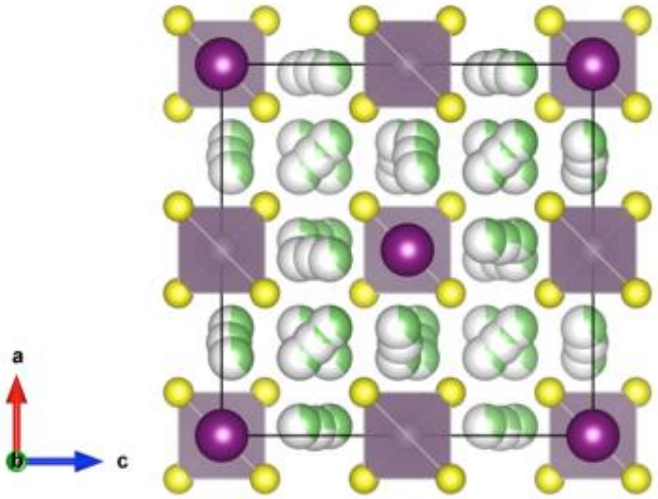

d) NASICON-like ($LiM_2(PO_4)_3$)

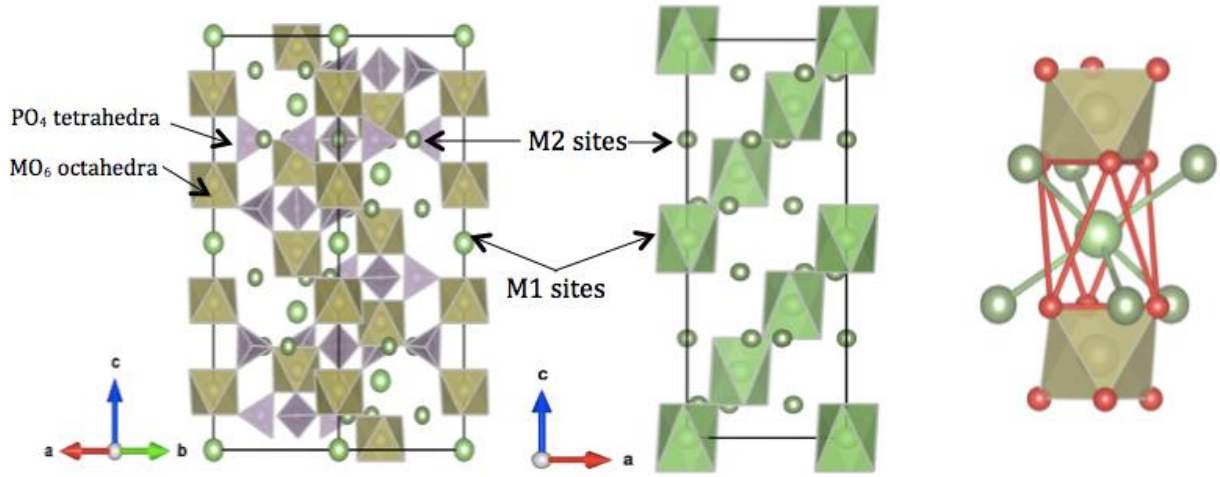

e) Garnet $A_3B_2(XO_4)_3$

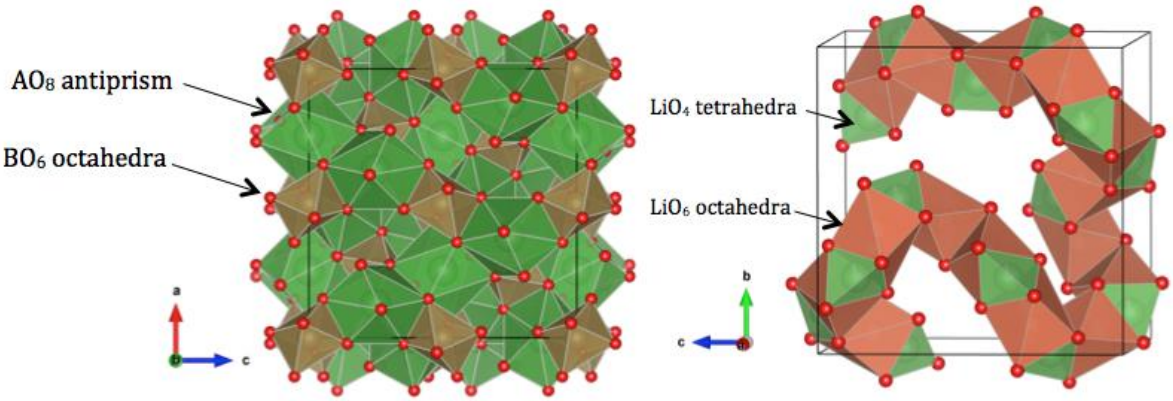

f) Perovskite

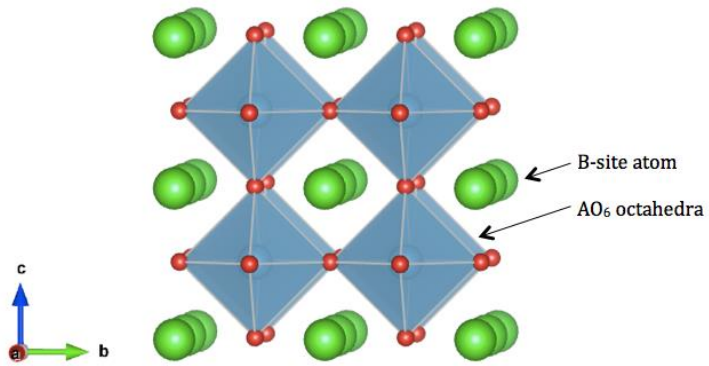

Figure S2. *Structural schematics of a) LISICON-like (the position of oxygen in the right panel is slightly displaced from their real position in order to emphasize the close packing of oxygen)., b)* $Li_{10}GeP_2S_{12}$*, c)argyrodite, d) NASICON-like, e) garnet and f) perovskite compounds.*

4. Supplementary Tables

Table S1. *Summary of measured temperature range, activation energy, pre-exponential factor, and extrapolation of conductivity to 300 K for Li-halides,[12-14] Li-nitrides,[15,16] Li-hydrides,[17,18] LISICON-like[19] in Figure 5 and LISICON-like[19] and NASICON-like[20,21] in Figure 9.*

		Range of temperature (K)	Activation energy (eV)	Pre-exponential factor (S/cm)	Conductivity extrapolated to 300 K (S/cm)	Reference
Li-Halide	Li_2CdCl_4	450-800	0.62	3.49E+04	1.20E-06	Lutz et al. 1981[12]
	Li_2CdI_4	350-495	0.73	3.12E+04	1.50E-08	Lutz et al. 1993[13]
	Li_2ZnI_4	320-416	0.63	8.67E+02	2.40E-08	Maekawa et al. 2008[14]
	Li_2MgCl_4	500-800	0.65	3.37E+04	3.21E-07	Lutz et al 1981[12]
Li-Nitride	$LiSi_2N_3$	415-730	0.64	1.24E+06	6.17E-08	Yamane et al. 1987[15]
	$LiPN_2$	370-600	0.72	2.60E+05	8.17E-10	Schnick et al. 1990[16]
Li-Hydride	$LiBH_4$	330-385	0.69	2.56E+06	3.00E-08	Matsuo et al. 2007[17]
	$LiNH_2$	320-400	0.86	2.30E+05	8.00E-10	Matsuo et al. 2010[18]
LISICON-like	$Li_{3.5}Si_{0.5}P_{0.5}O_4$	323-573	0.49	2.29E+01	1.31E -07	Deng et al. 2015[19]
NASICON-like	$LiHf_2(PO_4)_3$	313-413	0.33	4.10E+00	1.29E-05	Aono et al. 1993[20]
	$LiTi_2(PO_4)_3$	332-472	0.48	4.58E+01	3.83E-07	Martinez-Juarez et al. 1998[21]
	$LiGe_2(PO_4)_3$	333-433	0.60	8.61E+01	6.62E-09	Martinez-Juarez et al. 1998[21]

Table S2. *Summary of measured temperature range, activation energy, pre-exponential factor, and extrapolation of conductivity to 400 K for Li-X displayed in Figure 11a and 11b from high-temperature ionic conductivities.*[22]

	Range of temperature (K)	Activation energy (eV)	Pre-exponential factor (S/cm)	Conductivity extrapolated to 400 K (S/cm)
LiF	400 - 1100	1.99	3.00E+06	2.69E-19
LiCl	400 - 900	1.47	2.51E+06	7.89E-13
LiBr	400 - 800	1.29	1.41E+06	8.17E-11
LiI	400 - 700	1.05	9.60E+05	5.83E-08

5. Supplementary Figures

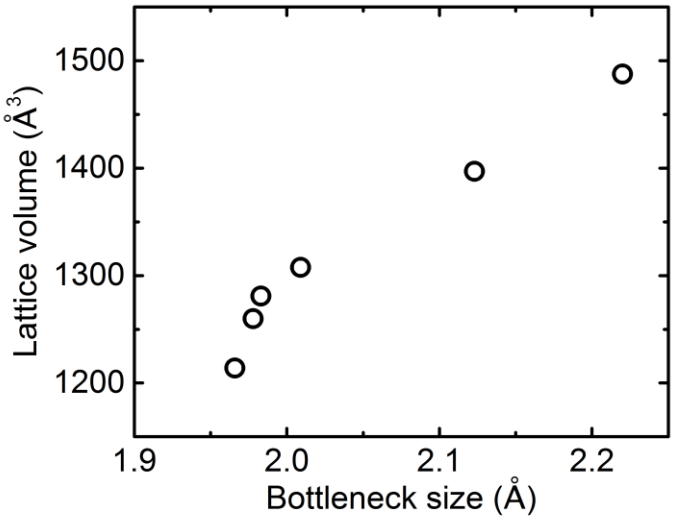

Figure S3. *Lattice volume as a function of bottleneck size for NASICON-like conductors in Figure 5b and Figure 7.*

References

(1) Linford, R. G.; Hackwood, S. Physical Techniques for the Study of Solid Electrolytes. *Chem. Rev.* **1981**, *81*, 327-364.

(2) Judeinstein, P.; Reichert, D.; Azevedo, E. R. d.; Bonagamba, T. J. NMR Multi-Scale Description of Ionic Conductivity Mechanisms Inside Polymer Electrolytes. *Acta Chim. Slov.* **2005**, *52*, 349-360.

(3) Shewmon, P. G. *Diffusion in Solids*; McGraw-Hill, 1963.

(4) Fritz, H. P.; Kuhn, A. Comparative Determination of Effective Transport Numbers in Solid Lithium Electrolytes. *J. Power Sources* **1993**, *41*, 253-261.

(5) Bruce, P. G.; Vincent, C. A. Steady State Current Flow in Solid Binary Electrolyte Cells. *J. Electroana. Chem. and Interfac. Electochem.* **1987**, *225*, 1-17.

(6) Evans, J.; Vincent, C. A.; Bruce, P. G. Electrochemical Measurement of Transference Numbers in Polymer Electrolytes. *Polymer* **1987**, *28*, 2324-2328.

(7) Bruce, P. G.; Evans, J.; Vincent, C. A. Conductivity and Transference Number Measurements on Polymer Electrolytes. *Solid State Ionics* **1988**, *28–30, Part 2*, 918-922.

(8) Zugmann, S.; Fleischmann, M.; Amereller, M.; Gschwind, R. M.; Wiemhöfer, H. D.; Gores, H. J. Measurement of Transference Numbers for Lithium Ion Electrolytes Via Four Different Methods, A Comparative Study. *Electrochim. Acta* **2011**, *56*, 3926-3933.

(9) Reinacher, J.; Berendts, S.; Janek, J. Preparation and Electrical Properties of Garnet-Type Li6BaLa2Ta2O12 Lithium Solid Electrolyte Thin Films Prepared by Pulsed Laser Deposition. *Solid State Ionics* **2014**, *258*, 1-7.

(10) Hebb, M. H. Electrical Conductivity of Silver Sulfide. *J. Chem. Phy.* **1952**, *20*, 185-190.

(11) Wagner, J. B.; Wagner, C. Electrical Conductivity Measurements on Cuprous Halides. *J. Chem. Phy.* **1957**, *26*, 1597-1601.

(12) Lutz, H. D.; Schmidt, W.; Haeuseler, H. Chloride Spinels: A New Group of Solid Lithium Electrolytes. *J. Phys. Chem. Solids* **1981**, *42*, 287-289.

(13) Lutz, H. D.; Zhang, Z.; Pfitzner, A. Fast Ionic Conductivity of Ternary Iodides in the Systems LiI-$M^{II}I_2$ (M^{II}=Mn, Cd, Pb). *Solid State Ionics* **1993**, *62*, 1-3.

(14) Maekawa, H.; Iwatani, T.; Shen, H.; Yamamura, T.; Kawamura, J. Enhanced Lithium Ion Conduction and the Size Effect on Interfacial Phase in Li_2ZnI_4–Mesoporous Alumina Composite Electrolyte. *Solid State Ionics* **2008**, *178*, 1637-1641.

(15) Yamane, H.; Kikkawa, S.; Koizumi, M. Preparation Of Lithium Silicon Nitrides And Their Lithium Ion Conductivity. *Solid State Ionics* **1987**, *25*, 183-191.

(16) Schnick, W.; Luecke, J. Lithium Ion Conductivity of $LiPN_2$ and Li_7PN_4. *Solid State Ionics* **1990**, *38*, 271-273.

(17) Matsuo, M.; Nakamori, Y.; Orimo, S.-i.; Maekawa, H.; Takamura, H. Lithium Superionic Conduction in Lithium Borohydride Accompanied by Structural Transition. *Appl. Phys. Lett.* **2007**, *91*, 224103.

(18) Matsuo, M.; Sato, T.; Miura, Y.; Oguchi, H.; Zhou, Y.; Maekawa, H.; Takamura, H.; Orimo, S.-i. Synthesis and Lithium Fast-Ion Conductivity of a New Complex Hydride $Li_3(NH_2)_2I$ with Double-Layered Structure. *Chem. Mater.* **2010**, *22*, 2702-2704.

(19) Deng, Y.; Eames, C.; Chotard, J.-N.; Lalère, F.; Seznec, V.; Emge, S.; Pecher, O.; Grey, C. P.; Masquelier, C.; Islam, M. S. Structural and Mechanistic Insights into Fast Lithium-Ion Conduction in Li_4SiO_4–Li_3PO_4 Solid Electrolytes. *J. Am. Chem. Soc.* **2015**, *137*, 9136-9145.

(20) Aono, H.; Sugimoto, E.; Sadaoka, Y.; Imanaka, N.; Adachi, G. y. Ionic Conductivity of Solid Electrolytes Based on Lithium Titanium Phosphate. *J. Electrochem. Soc.* **1990**, *137*, 1023-1027.

(21) Martínez-Juárez, A.; Pecharromán, C.; Iglesias, J. E.; Rojo, J. M. Relationship between Activation Energy and Bottleneck Size for Li^+ Ion Conduction in NASICON Materials of Composition $LiMM'(PO_4)_3$; M, M' = Ge, Ti, Sn, Hf. *J. Phys. Chem. B* **1998**, *102*, 372-375.

(22) Haven, Y. The Ionic Conductivity of Li-Halide Crystals. *Recl. Trav. Chim. Pays-Bas* **1950**, *69*, 1471-1489.